

Picoplanktonic methane production in eutrophic surface waters

Sandy E. Tenorio^{1,2,4}, Laura Farías^{1,2,3}

¹Departamento de Oceanografía, Facultad de Ciencias Naturales y Oceanográficas, Universidad de Concepción, Concepción, 4070043, Chile.

²Centro de Ciencia del Clima y la Resiliencia (CR2), Chile.

³Instituto Milenio en Socio-ecología Costera (SECOS), Chile.

⁴Programa de Graduados en Oceanografía, Departamento de Oceanografía, Universidad de Concepción, Concepción, 4070043, Chile.

Correspondence to: Laura Farías (laura.farias@udec.cl)

Abstract. Over the past decade, extensive research has delved into the methane (CH₄) paradox which involves aerobic CH₄ production. We present noteworthy observations of CH₄ oversaturation within the surface layer of the central Chile upwelling zone (36° S, 73° W) over two consecutive seasonal cycles (2018-2021). Complementing these observations, CH₄ cycling experiments were conducted, utilizing distinct plankton fractions (encompassing the natural planktonic community, fractions <150 μm, <3 μm, and <0.2 μm), in different productivity periods of phytoplanktonic production/composition throughout the year. Our findings underscore the pivotal role of picoplankton (<3 μm) in CH₄ production on the ocean surface, contrasting with the limited contribution of larger microorganisms (<150 μm). Notably, incubations with methylated substrates, such as methylphosphonic acid (MPn) and trimethylamine (TMA), induce heightened CH₄ production within the picoplanktonic fraction. This phenomenon is consistently observed during both upwelling (austral spring-summer) and non-upwelling (winter) seasons, with significance in the latter period, when *Synechococcus sp.* exhibits notably high relative abundance. Long-term microcosm experiments highlight the crucial roles played by heterotrophic bacteria and cyanobacteria in methylotrophic methanogenesis. This process enhances CH₄ production, facilitated by the recycling of dissolved organic carbon (DOC). Picoplankton emerges as a pivotal factor influencing the recycling of methylated substrates, and it is responsible for maintaining CH₄ supersaturation. These findings provide valuable insights into the biogeochemical processes driving CH₄ dynamics, particularly in highly productive upwelling areas.

Key words: dissolved methane, surface methane production, picoplankton, coastal upwelling.

Key points:

1. Picoplankton plays a crucial role in maintaining CH₄ supersaturation in the surface layer under different oceanographic conditions, influencing its exchange with the atmosphere.
2. Methylated substrates, such as methylphosphonic acid (MPn) and trimethylamine (TMA), notably stimulate CH₄ production through picoplankton-mediated methylotrophic methanogenesis.
3. *Synechococcus sp.*, utilizing the MPn substrate during the non-upwelling season, and picoeukaryotes, utilizing the TMA substrate during the onset of upwelling, could emerge as crucial microorganisms involved in CH₄ generation.

38 1. Introduction

39 Methane (CH₄) is a short-lived yet potent greenhouse gas, exhibiting a significantly higher heat-trapping capacity than CO₂
40 over a century. Its importance lies in its substantial influence on global climate dynamics and the necessity for robust mitigation
41 strategies (IPCC, 2021; Harmsen et al., 2020). The ocean holds considerable amounts of dissolved and hydrate CH₄, rendering
42 its thorough study crucial for precise climate change modelling and comprehending its ecological diversification within
43 oceanic ecosystems (IPCC, 2021; Xu et al., 2022).

44 The distribution of CH₄ is intricately influenced by both complex physical (transport) and biogeochemical (production and
45 consumption rates) processes (Reeburgh, 2007). In the open ocean, surface waters generally display slight oversaturation,
46 whereas deeper waters tend toward equilibrium or undersaturation with respect to the atmosphere. However, there is often
47 CH₄ accumulation within the pycnocline (Lamontagne et al., 1973; Cicerone and Oremland, 1988; Holmes et al., 2000). These
48 distribution patterns led to the identification of the CH₄ paradox (see review Reeburgh, 2007). Early hypotheses have suggested
49 various sources for CH₄ oversaturation in the surface layer, including organic matter respiration within anoxic niches of
50 particulate organic material (Karl and Tilbrook, 1994), within fish (Oremland, 1979), and zooplankton guts (De Angelis and
51 Lee, 1994). However, these classical methanogenesis pathways remain obscured in the surface and oxic zone of aquatic
52 systems. Subsequent advancements in this field highlighted biochemical processes, such as methylotrophic methanogenesis,
53 now understood as the production of CH₄ from methylated compounds under diverse biogeochemical conditions (Karl et al.,
54 2008; Damm et al., 2010, 2015; Repeta et al., 2016).

55 Methylated compounds are synthesized or degraded by diverse autotrophic and heterotrophic microorganisms, for example,
56 *Nitrosopumilus maritimus* produces phosphonates like methylphosphonic acid (MPn) (Metcalf et al., 2012), whereas different
57 species of phytoplankton, in turn, contribute to sulphur derivatives such as methionine (Lenhart et al., 2016),
58 dimethylsulfoniopropionate (DMSP), dimethyl sulfide (DMS) (Belviso et al., 1990; Stefels and Van Boekel, 1993) and
59 trimethylamines (TMA) (Sun et al., 2019), serving as potential carbon sources for microorganisms and thereby contributing
60 to CH₄ generation via methylotrophic methanogenesis. Furthermore, there is a suggestion that photosynthesis plays a role in
61 direct CH₄ production (Berg et al., 2014; León-Palmero et al., 2020; Klintzsch et al., 2023). Several studies have shown
62 associations between CH₄ anomalies in surface waters and specific phytoplanktonic groups, such as coccolithophores (Lenhart
63 et al., 2016) and cyanobacteria (Bizić et al., 2020). Hence, recognizing phytoplankton in various size fractions as direct links
64 to CH₄ production in diverse marine ecosystems (Bizić, 2021), becomes imperative, especially through pathways involving
65 demethylation from methylated compounds (Damm et al., 2010; Florez-Leiva et al., 2013; Lenhart et al., 2016; Karl et al.,
66 2008; Sun et al., 2011; Repeta et al., 2016).

67 Coastal upwellings, due to their high productivity, represent an emblematic site for the study of CH₄ production, but the
68 proximity to anoxic sediments and prevalent anaerobic methanogenesis in sediments or in the oxygen minimum zones (OMZ)
69 often obscures the study of CH₄ generation within oxygen-rich surface waters. Indeed, CH₄ profiles predominantly exhibit
70 significant increases towards anoxic sediments (Fariás et al., 2021; Ma et al., 2020; Kock et al., 2008). Coastal regions serve

71 as intensive CH₄ sources, facilitating lateral transport to open waters (Borges and Abril, 2012; Upstill-goddard and Barnes,
72 2016) and/or the atmosphere due to vertical advection linked to coastal upwelling (Fariás et al., 2021; Kock et al., 2008).
73 Current global CH₄ balances exhibit high uncertainty (Saunois et al., 2020; Roth et al., 2022; Lu et al., 2021) and considerable
74 spatial/temporal variability, particularly in coastal environments, where fluxes represent over 40% of total atmospheric fluxes
75 (Weber et al., 2019; Bange et al., 1994).

76 Given the upwelling systems are expected to integrate all before mentioned mechanisms, investigating CH₄ dynamics becomes
77 pivotal. Upwelling processes dynamically transport nutrient-rich water onto continental shelves and surface, significantly
78 enhancing biological productivity to eutrophic levels. This surge in high microbial productivity, biomass, and organic matter
79 decomposition, establishing these areas as pivotal hubs for carbon cycling, particularly in CH₄ (Capone and Hutchins, 2013).
80 Indeed, in upwelling systems a large part of the primary production is channelled to dissolved organic carbon (DOC) through
81 the microbial food web, and a less percentage directly to copepods via the herbivore food chain (Vargas et al., 2007). In
82 addition, coastal areas receive large amounts of DOC from rivers (Bianchi, 2011), this is also the case of upwelling systems
83 off central Chile (Vargas et al., 2013). These microbial food web and riverine pathways not only transport and remineralize
84 nutrients and DOC but also fosters the generation of greenhouse gases like CH₄ (Dinasquet et al., 2018; Sun et al., 2019).

85 Crucially, specific microbial groups such as Pelagibacter, SAR 11, among other, considered key players in DOC recycling,
86 have been identified as potential contributors to CH₄ regeneration from diverse C-1 compounds (Carpenter et al., 2012; Repeta
87 et al., 2016; Sun et al., 2019). The synergy between autotrophic (e.g., picoeukaryotes, cyanobacteria) and heterotrophic
88 picoplankton (<3 µm) could represent pathways for CH₄ production in coastal regions. Therefore, the main aim of this study
89 is to investigate the dynamics of CH₄ oversaturation within the surface layer of the central Chile upwelling zone using
90 observational and experimental approaches. Among objectives are to discern the contributions of different plankton fractions,
91 particularly picoplankton and to unravel the involvement of methylated substrates like MPn and TMA in stimulating CH₄
92 production. Ultimately, this research will provide comprehensive insights into the biogeochemical mechanisms that drive CH₄
93 dynamics within highly productive upwelling water, emphasizing the role of picoplankton in maintaining CH₄ oversaturation
94 in the surface ocean.

95 **2. Material and methods**

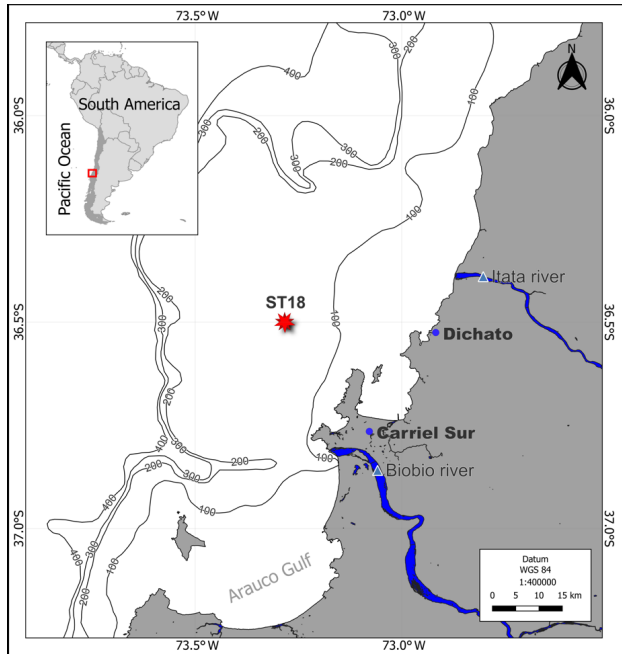
96 **2.1 Regional setting.**

97 The continental shelf off central Chile undergoes wind-driven coastal upwelling, seasonally controlled by the migration of the
98 South Pacific anticyclone (Strub et al., 1998). This process leads to alongshore equatorward winds during the summer- spring
99 period, producing coastal upwelling (Sobarzo and Djurfeldt, 2004; Sobarzo et al., 2007). The area is influenced by Equatorial
00 Subsurface Water (ESSW), which is nutrient rich and has low dissolved O₂ levels (less than 44 µM). The ESSW interacts with
01 sediments and serves as a nutrient source during coastal upwelling, delivering low O₂ concentrations and high organic matter

02 content to the bottom water and sediments, fostering anaerobic organic matter mineralization supporting denitrification,
03 sulphate reduction and methanogenesis (Ferderlman et al., 1997; Fariás et al., 2004).

04 2.2 Water collection.

05 Seawater was collected from the upwelling zone of central Chile ($36^{\circ} 08.02' S$; $73^{\circ} 07.750' W$) at the University of
06 Concepcion's time series station (ST18), situated at a depth of 90 meters (Fig. 1). Monthly samplings have been conducted
07 aboard the RV Kay Kay II since 2002. Continuous sampling with a CTD-O (SBE-19) instrument was performed to obtain
08 temperature, salinity, and dissolved oxygen (DO) profiles, whereas seawater samples using 10 L Niskin bottles at various
09 depths (0, 5, 10, 20, 30, 50, 65 and 80 m) were obtained in triplicate for dissolved gas (DO and CH_4), nutrient and chlorophyll-
10 a (Chl-a) analysis. Detailed methodologies can be found in Fariás et al. (2021). From March 2019 to June 2020, DOC samples
11 were specifically procured from depths of 5, 20, 50 and 80 m.



12
13 **Figure 1. Time series location map (ST18) over the central Chile upwelling platform. The Itata and Biobio rivers, Carriel sur**
14 **meteorological station and Dichato town are indicated.**

15 To investigate the role of different sized planktonic communities in CH₄ cycling, seawater was gathered at a depth of 10 m,
 16 a depth commonly associated with the Chl-a peak (Testa et al., 2018). Large zooplankton (150 µm mesh sieve) were excluded
 17 using the methodologies outlined by Sieburth et al. (1978). The experimental setup is outlined in Table 1 and includes two
 18 negative controls: 1) sterile filtration using a 0.2 µm filter, often-used method for the removal of microorganisms (Hahn, 2004),
 19 and 2) poisoning with the addition of HgCl₂ to ensure total inactivation of few bacterial species which can pass through 0.2-
 20 microm filters (Hahn, 2004). The positive control was the natural community (NC) without any filtration.

21 Another set of experiments enriched with the organic methylated substrates, MPn and TMA were performed using only the
 22 fractioned picoplanktonic community. To maintain the integrity of the samples, seawater was transported in dark and
 23 refrigerated drums placed inside expanded polystyrene boxes surrounded by ice packs to preserve the natural temperature of
 24 the seawater (~13°C) and minimize microbial activity. The average time for transportation to the Marine Station Biology
 25 Laboratory at Dichato was approximately 4 hours. However, it is important to note that there were delays of 8 to 12 hours
 26 between arrival at the laboratory and the onset of short- and long-term experiments, respectively. These delays were due to
 27 filtering and a short acclimatization process (6 hours) required before initiating the experiments, but these procedures were
 28 done in cool room (13°C).

29 This is a time series study, from 2018 until 2021, encompassing CH₄ regeneration in different productivity phases (Table 1)
 30 according to (Testa et al., 2018). In this regard, two types of experiments described in the following sections will be conducted.

31 **Table 1. Summary of the experimental setup of short-term (GC vials) and long-term (microcosms) experiments with different**
 32 **treatments: NC: seawater with the natural plankton (control); <3 µm: picoplankton; <0.2 µm: femtoplankton (control +); <0.2 µm**
 33 **+ HgCl₂: femtoplankton with HgCl₂ (control +) and CC: picoplankton concentrate; and the addition of methylated substrates (MPN:**
 34 **methyl phosphonic acid and TMA: trimethylamines). Different phases of the productivity period are: PI: Phase I; PII: Phase II;**
 35 **and PIII: Phase III.**

Deleted: as

Deleted: the seawater was transported in light- restricted black drums under controlled temperature conditions to the Marine Station Biology laboratory at Dichato, minimizing the potential for biological activity. ...

Date	Type of experiment	Setup	Plankton size (µm)	Place	Time (h)	Productivity period
December 2018	GC vials	Plankton fractionation	CN, <3 and <0.2	Incubator	24	High (PI)
January 2019	GC vials	Plankton fractionation	CN, <3 and <0.2	Incubator	24	High (PI)
March 2019	GC vials	Add: MPn	<3	Incubator	24	Intermediate (PII)
May 2019	GC vials	Add: MPn and TMA	<3	Incubator	24	Basal (PIII)

April 2019	Microcosms	Add: MPn and TMA	CN, <3, and CC	Cold room	~ 60	Intermediate (PII)
September 2019	Microcosms	Add: MPn and TMA	CN, <3, and CC	Cold room	~ 60	High (PI)

41

42 **2.3 Short-term experiments of CH₄ cycling from size-fractionated planktonic community enriched with organic**
43 **substrates.**

44 The size fractionation of planktonic communities was conducted through a careful sequential filtration process, where 5 L of
45 seawater was gently passed through a pre-filter of 150 µm nylon, followed by 3 µm Isopore, and 0.22 µm Millipore membranes,
46 yielding two fractions: picoplankton (<3 µm), and femtoplankton (<0.2 µm) communities; the last one used as a negative
47 control in some experiments. NC was obtained directly without filtering (Table 1).

48 Prior to incubation, initial seawater sampling was taken for each treatment group, wherein triplicate measurements were taken
49 of PO (125 mL), COD (60 mL), Chl-a (100 mL), and nutrients (15 mL). Subsequently, each size-fractionated sample was

50 homogenized and swiftly transferred into 20 mL vials (108 in total, twenty-seven per treatment). These vials were immediately
51 sealed using rubber and aluminium caps to prevent any potential atmospheric gas contamination. The incubation of these vials
52 took place within an FOC 225E incubator, maintained at a temperature of 13 °C, and under a 12-hour photoperiod (24 hours).

53 The illumination was calibrated to fall in a range of 11-11.5 µmol m⁻² s⁻¹ using blue and neutral density blank filters. At
54 intervals of four hours, three vials from each treatment (Table 1) were withdrawn, and immediately poisoned with 50 µL of

55 HgCl₂ and then, the vials were gently agitated to ensure homogenization. Gas chromatography was employed to analyze the
56 CH₄ content of the vials. In another set of experiments (Table 1), the picoplankton fraction was singled out to ascertain its

57 capacity for metabolizing methylated substrates and subsequently regenerating CH₄. This involved adding MPn and TMA to
58 the samples. The final concentration of both substrates in these treatments was maintained at 1 µM, assuming that natural

59 concentrations in the seawater were at trace levels. Thus, these could be considered as potential experiments (highly enriched).

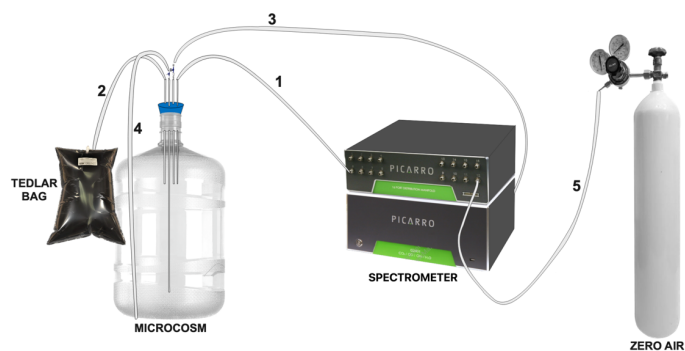
60 The experimental conditions remained consistent with those employed in the earlier experiment.

61 **2.4 Long-term experiments of CH₄ cycling from size-fractionated planktonic community enriched with organic**
62 **substrates.**

63 Nine microcosms were developed using a system of gas-tight polycarbonate bottles (13 L). Each microcosm contained 10L of
64 seawater for treatment and 3L of headspace. They were equipped with a closed gas circuit and connected to a gas spectrometer
65 analyzer capable of simultaneously and continuously measuring various gases, including CO₂, CH₄, N₂O, and humidity
66 percentage (Fig. 2). Each bottle featured a rubber cap equipped with four holes (as depicted in Fig. 2), housing a 5mm glass
67 capillary within each hole. These capillaries were connected to gas-tight Teflon hoses. Specifically, the first capillary extended

Deleted: OD

69 to the middle of the headspace (1) and was linked to an accessory (16-Port Distribution Manifold A0311) of the Picarro G-
70 2308 spectrometer for Cavity Ring Spectroscopy System (CRDS), designed for the measurement of gases in equilibrium with
71 the aqueous phase. The second capillary was suspended within the headspace (2) and connected to a Tedlar bag (3 L) filled
72 with N₂. This arrangement aimed to prevent imbalance when drawing water samples from the microcosm. The third capillary,
73 also suspended in the headspace (3), was equipped with a 3-way cannula, and was connected to the air outlet of the Picarro G-
74 2308 spectrometer, to facilitate the recirculation of air within the headspace. This system optimization aimed to mitigate
75 excessive headspace during spectrometer air sampling, preventing a gas-seawater phases imbalance. This hose (3) was
76 adjustable and replaced upon measuring gas concentrations in each microcosm. The fourth glass capillary was submerged in
77 the seawater, 3 cm from the bottom (4). It was attached to a 3-way cannula, streamlining the sample extraction process.



78
79 **Figure 2. Assembly of the microcosm for long-term experiments (10 L). Capillary 1 is connected directly to the spectrometer.**
80 **Capillary 2 is connected to a TEDLAR bag filled with N₂ (3L). Capillary 3 is removable and connected to the outlet of the**
81 **spectrometer. Capillary 4 is connected to a loose hose for water sampling and hose 5 is connected to zero air.**

82 In both April and September of 2019, a series of long-term microcosm experiments were conducted. These months were
83 strategically chosen: the first coinciding with the transition of phytoplankton composition to nano-picoplankton (basal
84 productivity period), and the second with diatom blooms (larger phytoplankton dominance) (high productivity period), as
85 highlighted in studies by Anabalón et al. (2007) and Cuevas et al. (2004). The experiment encompassed three distinct
86 treatments, 1) Control without any methylated substrates addition in natural communities (NC), picoplankton community (<
87 3 μm) and concentrated picoplanktonic community (CC) 2) all treatments enriched with MPn 3) and all treatments enriched
88 with TMA (see Table 1).

89 The concentrated fraction of picoplankton (CC) was procured through tangential flow filtration via a 0.2 μm filter, following
90 a procedure developed by Giovannoni et al. (1990) for harvesting greater quantities of microbial biomass and using pre-

91 filtering steps as discussed earlier to concentrate only picoplankton (<3 µm). To discern whether the tangential flow filtering
92 was effective, the abundance of cyanobacteria, picoeukaryotes and heterotrophic bacteria was measured with flow cytometry.
93 The incubations were carried out within a controlled cold room environment, maintaining a temperature range of 12 to 13 °C,
94 with same illumination used in short periods over 60 hours. In the initial stages, each bottle was sealed and allowed to acclimate
95 for six hours in darkness. Following this stage, 1 mL of MPn (10 mM stock solution) and TMA (10 mM stock solution) were
96 introduced to each bottle, yielding a final concentration of 1 µM, matching the conditions established in prior experiments.
97 To prevent CH₄ residue contamination, a purge with Zero air was performed (as shown in Fig. 2, line 5), ensuring accurate
98 CH₄ concentration measurement within each microcosm, and establishing a baseline. Every four hours a cycle of CH₄
99 measurements was conducted continuously over 3 minutes, followed by a 6-minute hose cleaning (used for recirculation) with
!00 Zero air before connecting to capillary 3 for subsequent measurement. It is important to note that the equipment absorbed 240
!01 mL of air per minute of reading. Therefore, air recirculation within the microcosm, as previously mentioned, was essential.
!02 Preceding the actual experiment, the concentrations of gases measured by the spectrometer were closely monitored for 30
!03 minutes, confirming that the recirculation process did not impact the measured gas concentrations.

!04 **2.5 Chemical and biological analysis.**

!05 **2.5.1. Dissolved methane.**

!06 Once the CH₄ samples were taken, they were stored upside down, at room temperature and protected from light, and then
!07 analyzed in the GC. CH₄ (discrete samples) was determined using the phase equilibrium method (McAuliffe, 1963). In this
!08 procedure, each vial was carefully treated, with the addition of 5 mL of inert gas (helium), creating a headspace to facilitate
!09 equilibrium between the aqueous and gas phases. Subsequently, the gas phase was measured into a gas chromatography
!10 Shimadzu 17 equipped with a flame ionization detector (FID). A Restek RT QS-Bond column (30 m length, 0.53 mm inner
!11 diameter, 20 µm film thickness) was employed, maintained at a temperature of 30 °C with a flow of 2.6 ml min⁻¹, using He as
!12 an ultrapure gas carrier.

!13 Five-point calibration curves (linear response of the detector) were made for each monthly sample set (treatment), using a gas
!14 with a composition and concentration equivalent to that of the current atmosphere from NOAA (1863.4 ± 0.3 ppbv for CH₄)
!15 (Bullister et al., 2016) as the primary standard, as well as three standard gas mixtures (Air Liquide, USA) and zero air (synthetic
!16 air without CH₄ tracers). In each CH₄ sample set (every treatment), standards were added at the beginning, middle and end of
!17 the measurements to corroborate the correct functioning of the detector. CH₄ measurements (triplicate) with a variation
!18 coefficient greater than 10% were not considered.

!19 **2.5.2. Dissolved oxygen.**

!20 To assess DO content, 125 mL glass flasks were used for sample collection in triplicate. These samples were immediately
!21 fixed and analyzed within 6 hours of collection through the Winkler method (Carpenter, 1965). The analysis was conducted

!22 using a Dosimat 665 instrument featuring an automatic photometric endpoint detector. The detection limit for this method
!23 stood at 2 $\mu\text{mol L}^{-1}$.

!24 **2.5.3. Nutrient.**

!25 Nutrient samples were collected in triplicate using a 60 mL syringe and filtered through a 0.45 μm cellulose acetate filter. The
!26 filtered content was held in 15 mL Falcon polyethylene bottles and stored at -20°C . Analysis of these nutrient samples followed
!27 standard colorimetric techniques (Grasshoff et al., 1983) and was conducted using a SealAA3 segmented flow auto-analyzer.
!28 This analyzer featured four distinct channels, each equipped with specific modules tailored for individual nutrients.

!29 **2.5.4. Chlorophyll-a.**

!30 To quantify Chl-a content, triplicate samples of 100 mL seawater were filtered using a GF/F filter and immediately stored at -
!31 20°C . Analysis was performed according to the method outlined by (Holm-Hansen et al., 1965). A Turner Designs 10AU
!32 fluorometer was employed for measurement, and a standard pigment served as a reference (Sigma-Aldrich C6144-1MG).

!33 **2.5.5. Dissolved Organic Carbon.**

!34 For DOC assessment, samples were collected in triplicate using polyethylene bottles. Each 60 mL seawater sample was filtered
!35 through a GF/F filter that had been pre-treated by heating at 450°C for 4 hours. After filtration, the samples were acidified to
!36 achieve a pH range of 2-3 and stored at -20°C . Analysis of these samples involved the infrared combustion method using a
!37 Shimadzu Organic Carbon Analyzer (TOC-LCPH).

!38 **2.5.6. Cytometry.**

!39 For picoplankton abundance, 3mL of water was fixed with a glutaraldehyde solution (1%) and promptly frozen (-80°C) in
!40 liquid nitrogen for storage. Samples were analyzed with flow cytometry using an INFLUX, Cytopeia, equipped with five lasers
!41 (355-457-488-532-638 nm). Sort gates were optimized based on the autofluorescence of each group. *Synechococcus sp.* were
!42 identified based on their orange fluorescence (530/40 nm) using 488 nm blue and 532 nm green lasers, picoeukaryotes were
!43 identified by their red fluorescence (692/40 nm) using 488 nm blue laser, and bacterioplankton were detected using a
!44 combination of side scatter light (SSC) (related to cell size) versus green fluorescence (530/40 nm).

!45 **2.6 Data analysis.**

!46 **2.6.1. Dissolved methane.**

!47 Dissolved CH_4 concentration was calculated using the solubility coefficient from Wiesenburg and Guinasso (1979). The water
!48 column was divided into two layers according to density gradients: (1) surface layer (0 - 20 m) well mixed and (2) subsurface
!49 layer (20 - 90m) from the base of the mixed layer to the bottom, around ~ 90 m (Farias et al., 2015), this was to interpret the
!50 vertical and temporal variability of CH_4 variation.

!51 [CH₄ dissolved in the microcosms were measured using continuous sampling connected to the spectrometer CRDS. To convert](#)
!52 [CH₄ concentrations from molar dry phase to dissolved concentrations the Wiesenburg and Guinasso \(1979\) solubility](#)

Deleted: the

!54 coefficient, calculated from the *in-situ* T and S, was used. Each time in the microcosm experiment represents the average of
!55 the plateau of each measurement (around 150 and 200 measurements, approximately).

!56 **2.6.2. Methane saturation.**

!57 CH₄ saturation was calculate following Eq. (1):

$$!58 \text{ Sat}(\%) = \frac{[CH_4]_{in\ situ}}{[CH_4]_{eq}} \quad (1)$$

!59 Where [CH₄]_{eq} was calculated using solubility coefficient from Wiesenburg and Guinasso (1979).

!60 **2.6.3. Methane anomalies and methane hot moments.**

!61 Monthly anomalies of CH₄, were estimated only in the surface layer, using the following Eq. (2):

$$!62 \text{ Anomaly} = \frac{xCH_4 - \bar{x}CH_4}{\sigma_{CH_4}} \quad (2)$$

!63 Where: xCH₄ is the discrete value at a certain depth (surface) and time (month), and $\bar{x}CH_4$ is the median value for the whole
!64 (2018-2021) period at surface and σ_{CH_4} is the standard deviation of this dataset. CH₄ hot moments were defined as a ΔCH_4
!65 three times higher than the average monthly of anomaly ($\bar{x} \Delta CH_4$) at each depth within the surface layer as Eq. (3):

$$!66 \frac{\Delta CH_4}{\bar{x} \Delta CH_4} > 3 \quad (3)$$

!67 Where: ΔCH_4 is the disequilibrium of this gas at each depth and was estimated as Eq. (4):

$$!68 \Delta CH_4 = [CH_4]_{in\ situ} - [CH_4]_{eq} \quad (4)$$

!69 **2.6.4. Inventories.**

!70 Inventories of CH₄, Chl-a and nutrients at the surface (**SL**) and **illuminated layer** and subsurface **and dark layer (SSL)** were
!71 calculate through the trapezoidal integration of concentrations of each variable at every layer; minimum three depths in each
!72 layer. The averages were taken for DOC, because there were only two measurements in each layer.

!73 **2.6.5. Methane recycling rates.**

!74 The net CH₄ recycling rate (net CH₄ accumulation minus CH₄ consumption) in different fractions of the phytoplankton
!75 community was calculated through a linear regression of CH₄ concentrations (Farias et al., 2009) during the incubation time
!76 (24 hours), separating the light cycles (12 hours of light and 12 hours of darkness).

!77 **2.6.6. Methane fluxes.**

!78 The daily CH₄ flux ($F = \mu\text{mol m}^{-2} \text{ d}^{-1}$) across air-sea interface was determined using the equation from Broecker and Peng
!79 (1974), modified by Wanninkhof (1992) as follows Eq. (5):

$$!80 F = K_w * (C_w - C^*) \quad (5)$$

!81 Where: K_w (cm h^{-1}) is the transfer velocity from the surface water to the atmosphere, as a function of wind speed, temperature,
!82 and salinity from the mixed layer depth (MLD), where wind speed were obtained from a meteorological station located at
!83 Carriel Sur (<http://www.meteochile.gob.cl/>) and MLD was calculated using a potential density-based criterion of Kara et al.
!84 (2003). C_w (nmol L^{-1}) is the mean CH₄ concentration in the mixed layer and C^* is the gas concentration in the mixed layer
!85 expected to be in equilibrium with the atmosphere according to Wiesenburg and Guinasso (1979). Historical atmospheric

!86 values were obtained from registers of gas hemispheric and global monthly means from the NOAA/ESRL program at NOAA
!87 (<http://www.esrl.noaa.gov>). More details about the calculation of CH₄ fluxes in Fariás et al. (2021).

!88 2.6.7. Brunt-Väisälä frequency (BVF).

!89 The Brunt Väisala frequency was derived from the observed pressures, temperatures and salinities for each depth set using the
!90 TEOS-10 equation of state. This was done in Ocean Data View (ODV v5.6.4) software. Negative values indicate unstable
!91 conditions (Schlitzer, 2023).

!92 2.7 Statical analysis

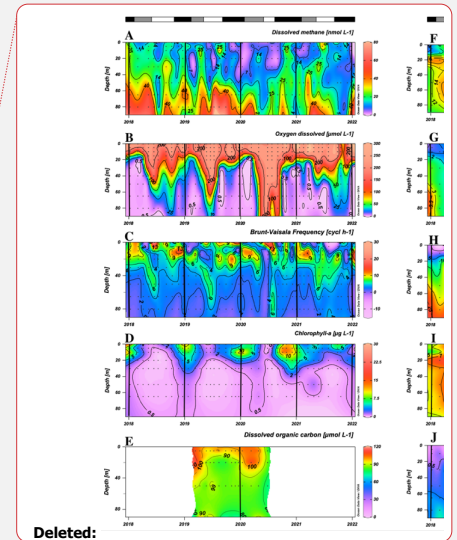
!93 To determine significant differences between the upwelling and non-upwelling periods in both surface and subsurface layers,
!94 the non-parametric Mann-Whitney U test was used. To analyse the degree of relationship between oceanographic variables
!95 and the variability of CH₄ in the surface layer, Spearman correlations were used. Also, to identify patterns surface and
!96 subsurface variation, a Principal Component Analysis (PCA) was performed. In addition, the Kruskal-Wallis non-parametric
!97 statistical test was used to define significant differences between the concentrations given by the different treatments. The
!98 value statistically significant was considered as $p < 0.05$.

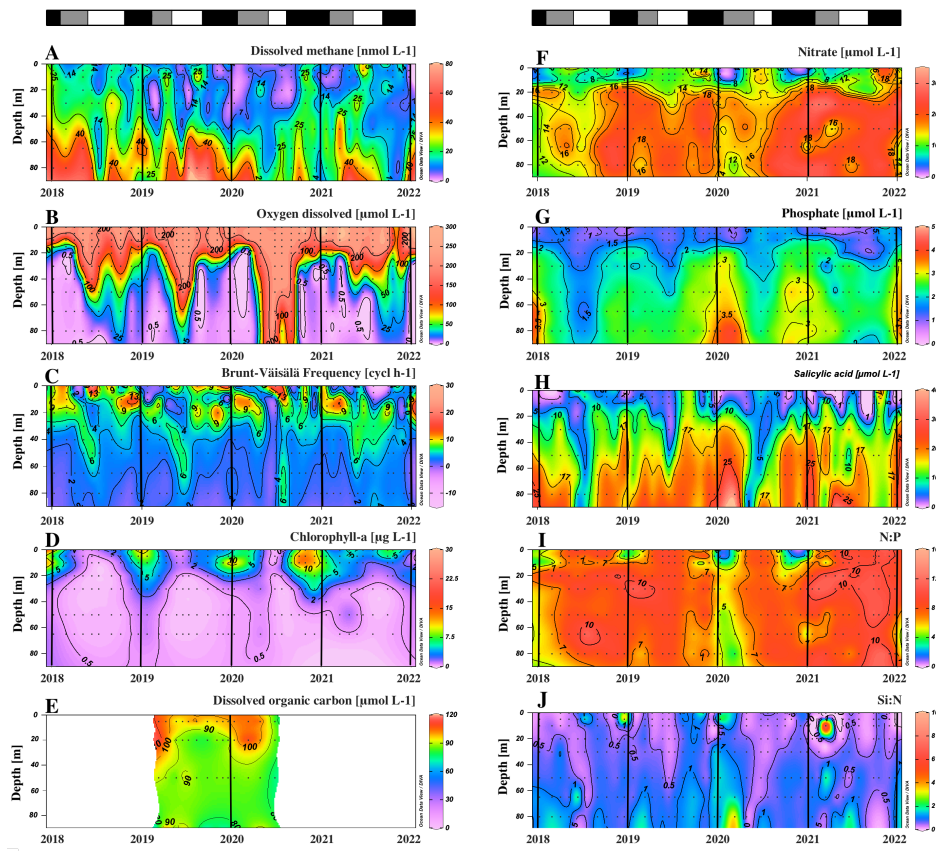
!99 3 Result and discussion

!00 3.1 Oceanographic characteristics related to wind-driven coastal upwelling in central Chile.

!01 Figure 3 shows the seasonal variability of DO, stratification, Chl-a, DOC, nutrients, and their ratios. Coastal areas off central
!02 Chile have a well-documented seasonality of upwelling favourable winds (Strub et al., 1998). Previous studies, based on wind
!03 forcing, have identified two distinct seasons: spring-summer (September to April) upwelling and fall-winter (May to August)
!04 non-upwelling (Sobarzo et al., 2007). This seasonality significantly influences temperature, salinity, DO, nutrients, and surface
!05 Chl-a concentrations in response to wind-driven stress (Strub et al., 1998; Aguirre et al., 2012). Notably, although most
!06 oceanographic variables have clear seasonal patterns, a comparatively weak seasonality is observed in dissolved CH₄ (Fig.
!07 3A).

!08





10
 11 **Figure 3.** Time series of vertical distributions of A. Methane (nmol L⁻¹), B. Dissolved oxygen (µmol L⁻¹), C. Brunt-Vaisala Frequency
 12 (cycl h⁻¹), D. Chlorophyll-a (µg L⁻¹), E. Dissolved Organic Carbon (no Purgeable Organic Carbon - µM), F. Nitrate (µmol L⁻¹), G.
 13 Phosphate (µmol L⁻¹), H. Salicylic acid (µmol L⁻¹), N:P ratio and J. Si:N ratio. Sampling was made at ST18 from January 2018 to
 14 December 2021. Black lines indicate the start of each year (January). The top bars show different periods primary production, in
 15 black is a high productivity period (Phase I), in gray is an intermediate productivity period (Phase II), and in white is a low
 16 productivity (Phase III).
 17

18 In the subsurface layer, CH₄ concentrations range from 0.43 to 78.72 nM (mean ± SD = 23.44 ± 15.38 nM, Fig. 3A). These
 19 elevated levels could be associated with the seasonal dynamics of organic matter mineralization under hypoxic and suboxic

i20 conditions during the upwelling period (spring-summer) (Brown et al., 2014; Capelle and Tortell, 2016; Kock et al., 2008;
i21 Farias et al., 2021); however, there are no significant differences in CH₄ accumulations ($p = 0.40$) in subsurface waters during
i22 the upwelling (mean \pm SD = 22.52 \pm 14.34 nM) and non-upwelling (mean \pm SD = 24.60 \pm 16.65 nM) periods (Fig. 3A).
i23 Previously, long-term CH₄ climatology has observed similar values in surface and subsurface layers (Farias et al., 2021).
i24 In the surface layer, there is a highly heterogeneous distribution of CH₄ concentrations, ranging from 0.14 to 41.72 nM (mean
i25 \pm SD = 11.70 \pm 7.79 nM). There are brief events of high CH₄ accumulations within water column, known as “hot moments”
i26 (McClain et al., 2003; referring to disproportionate accumulations over time). CH₄ concentrations during hot moments are
i27 between 10.17 nM (390% saturation) and 41.72 nM (1650% saturation) and persist during upwelling and non-upwelling
i28 periods, as observed in Fig. S1 and Fig. S2. Persistently high CH₄ concentrations in mixing layer depth results in substantial
i29 CH₄ effluxes, varying between 3.35 and 23.42 $\mu\text{mol m}^{-2} \text{d}^{-1}$ (mean \pm SD = 10.10 \pm 5.77 $\mu\text{mol m}^{-2} \text{d}^{-1}$). When effluxes are
i30 estimated and compared for upwelling and non-upwelling periods, there are not significant differences. The lack of seasonal
i31 differences in mean surface CH₄ concentrations ($p = 0.63$) and effluxes ($p = 0.23$) could indicate additional input sources, such
i32 as river discharges or local surface production. Potentially, the Itata River may contribute to CH₄, DOC and chromophoric
i33 DOM (CDOM) discharge (Bello, 2016; Vargas et al., 2016; Rain-Franco et al., 2019); stimulating CH₄ production through
i34 aerobic methanogenesis and photooxidation processes (Li et al., 2020; Zhang and Xie, 2015).
i35 CH₄ profiles from samples are shown in Figure S2. Specific dates present peaks in surface CH₄ over different concentrations,
i36 occasionally presenting levels exceeding those in the subsurface layer; so, it is understood that these hot moments in the surface
i37 layer are not associated with the vertical advection of CH₄-rich bottom waters.
i38 Thus, it is considered whether hot moments result from physical processes, such as vertical and/or advection associated with
i39 upwelling and river discharge, respectively, or biological microbial processes. For the latter, hot moments might be due to *in*
i40 *situ* aerobic methanogenesis, a process related to the growth and metabolic activities of microalgae (Günthel et al., 2020;
i41 Hartmann et al., 2020; Del Valle and Karl, 2014; Bizic, 2021; Cerbin et al., 2022) and bacteria (Repeta et al., 2016; Metcalf
i42 et al., 2012; Sun et al., 2019). This type of production is suggested to be a significant reason for CH₄ fluxes in various aquatic
i43 systems, including stratified lakes (Grossart et al., 2011; Günthel et al., 2019; Wang et al., 2018), and open oceans (Damm et
i44 al., 2010; Karl et al., 2008; Repeta et al., 2016; Sosa et al., 2020; Ye et al., 2020).
i45 Relatively high Brunt-Väisälä frequency (BVF) values (>10 cycl/h) are observed between depths of 0 and 20 m, particularly
i46 from September to December (Fig. 3C), whereas subsurface BVF values seem to be associated with annual patterns of thermal
i47 stratification, where upwelling from the nearly homogenous ESSW between October and April leads to high density
i48 homogeneity and lower BVF values. During fall and winter, elevated BVF values are observed in surface waters, probably
i49 due to discharge from the Itata river; remarkably there are notably stable values in the subsurface layer (Fig. 3C).
i50 The upper 20 m of the water column has Chl-a concentrations above 10 $\mu\text{g L}^{-1}$ (with a marked subsurface peak over different
i51 depths) (mean \pm SD 6.60 \pm 5.98) in September to January (spring-summer); while lower and more homogeneous values
i52 (ranging from 0.5 to 1 $\mu\text{g L}^{-1}$) are detected during late summer (February to April, mean \pm SD 3.23 \pm 2.87), fall and winter
i53 (May to August, mean \pm SD 1.36 \pm 1.91) (Fig. 3D). The study area presents typical DOC concentrations, as expected for

highly productive coastal zones (Igarza et al., 2019; Vargas et al., 2013), ranging from 58.79 to 128.63 μM (mean \pm SD = 90.37 ± 17.05) with peak DOC concentrations during late summer and early fall (Fig. 3E). The surface layer shows reduced, but not depleted nutrient concentrations, whereas the subsurface layer presents consistently higher nutrient concentrations (Fig. 3F–H). Within the upper 10 m depth, minimum mean NO_3^- and PO_4^{3-} concentrations occur from September to January, and intermediate and higher values between February and August (Fig. 3 F-G). These trends are consistent with plankton temporal dynamics (see below). In contrast, Si(OH)_4 exhibits higher but heterogeneous concentrations during late autumn and winter, and lower values during spring and summer (Fig. 3H). This pattern reflects the high levels of Si(OH)_4 associated with river discharges in winter and the development of diatom blooms in spring and summer. CH_4 hot moments occur consistently throughout the year with different stratification scenarios in the water column (Fig. 3A and C), and with different Chl-a levels (Fig. 3D), revealing a complex interaction between substrates (nutrients and DOC), involved microorganisms and environmental factors (e.g. light, nutrients, water column stability).

Three distinct periods or phases of annual productivity are considered within the study area, based on existing data of primary production, phytoplankton biomass, and phytoplankton succession (i.e. changes in composition), related with other biophysical variables (Testa et al., 2018). These periods are; September to January (Phase I), with high productivity and Chl-a biomass, dominated by microplankton including large diatoms, tintinids, and dinoflagellates; from February to April (Phase II) with intermediate productivity, characterized by a shift in plankton composition biomass from larger to smaller organisms, such as flagellates; and from May to August (Phase III), with basal level productivity and relatively low Chl-a biomass, which corresponds to a non-upwelling period, with a prevalence of pico and nanoplankton (e.g., *Synechococcus*) including small flagellates and ciliates.

Table 2 presents inventories on CH_4 , Chl-a, DOC, NO_3^- , PO_4^{3-} , Si(OH)_4 , and inorganic nutrient ratios (N:P and Si:N) observed in these periods. The data on Chl-a indicates a marked variation, decreasing from spring to winter (Table 2).

Table 2. Average inventories of biogeochemical variables: methane ($\mu\text{mol m}^{-2}$), chlorophyll-a (mg m^{-2}), DOC ($\mu\text{mol m}^{-2}$), nitrate ($\mu\text{mol m}^{-3}$), phosphate ($\mu\text{mol m}^{-3}$), silicate ($\mu\text{mol m}^{-2}$), N:P and Si:N ratios, estimated for each productivity period (mean \pm SD) from 2018 to 2021. These inventories are estimated for surface layer (SL) and subsurface layer (SSL). Number of hot moments in each period are counted. Phase I: September to January. Phase II: February to April. Phase III: May to August.

Formatted: English (UK)

Variable	Layer	Productivity periods		
		High	Intermediate	Basal
		Phase I (spring-summer)	Phase II (summer-autumn)	Phase III (autumn-winter)
CH_4	SL	265.59 \pm 58.36	162.35 \pm 21.44	240.54 \pm 78.97
	SSL	1315.07 \pm 173.69	1012.86 \pm 163.23	1275.17 \pm 286.38
Chl-a	SL	154.4 \pm 102.31	51.32 \pm 31.02	26.19 \pm 21.17
DOC	SL	114.44 \pm 53.94	112.88 \pm 8.36	92.41 \pm 11.27

	SSL	100.35 ± 46.51	96.97 ± 23.78	86.12 ± 8.95
NO ₃ ⁻	SL	260.61 ± 96.25	208.67 ± 49.51	224.65 ± 13.44
	SSL	1274.41 ± 344.24	1033.51 ± 38.5	987.6 ± 113.58
PO ₄ ⁻³	SL	38.08 ± 10.35	30.29 ± 3.51	28.16 ± 2.99
	SSL	170.22 ± 34.07	137.05 ± 21.57	119.38 ± 11.73
Si(OH) ₄	SL	131.75 ± 47.07	91.65 ± 38.68	111.24 ± 37.9
	SSL	1065.32 ± 206.98	811.2 ± 225.51	678.07 ± 168.68
N:P	SL	7.69 ± 2.57	7.59 ± 2.44	8.48 ± 0.55
	SSL	9.28 ± 2.52	8.24 ± 0.92	8.46 ± 0.84
Si:N	SL	0.67 ± 0.1	0.69 ± 0.73	0.49 ± 0.15
	SSL	1.04 ± 0.08	1.01 ± 0.26	0.74 ± 0.11
Hot moments	SL	19	9	15

79
 80 Notably, surface data on DOC shows a marginal reduction from Phase I to Phase III (Table 2). It is possible that this fluctuation
 81 in DOC accumulation/depletion is due to the microbial regeneration exceeding the heterotrophic bacterial consumption
 82 (Hansell and Orellana, 2021), or it attributes to allochthonous sources from rivers (Bauer and Druffel, 1998). Nutrient
 83 distribution and concentrations in the surface layer show significant variability among phases (Fig. 3F, G, and H) due to the
 84 varied influence by nutrient-rich upwelling events (predominantly observed in spring-summer), biological assimilation and
 85 river discharge. These variations significantly affect the N:P and Si:N ratios (Fig. 3I and J), potentially influencing
 86 phytoplankton composition. During winter (Phase III), the N:P ratio approaches the expected Redfield stoichiometry, attributed
 87 to reduced denitrification in bottom waters (Fernandez et al., 2015) and limited vertical advection towards the surface,
 88 contrasting with Phase I. Simultaneously, the Si:N ratio increases due to freshwater discharge from the Itata River (Phase III),
 89 encouraging an increase in large diatoms and subsequent Si(OH)₄ consumption (Phase I). Considering that hot moments occur
 90 throughout different phases and stages of primary production, as well as phytoplankton composition succession (Collado-
 91 Fabbri et al., 2011; Aldunate et al., 2018; Anabalón et al., 2007), various levels of Chl-a a (see Table 2), and under different
 92 nutrient ratios and DOC concentrations (Table 2), it suggests that the conditions and processes favouring the occurrence of hot
 93 moments are variables and not entirely clear.

94 The correlation analysis in the water column showed no significant correlations between CH₄ and the other physicochemical
 95 variables (Fig. S3A), however nutrients such as PO₄⁻³ were significantly correlated with T (negative correlation), S (positive
 96 correlation), DO (negative correlation) and Si:N ratio (positive correlation) (Fig. S3A), which may be associated with the
 97 nutrient-rich, oxygen-poor of the ESSW. When the surface layer was analyzed in the three productivity periods (Fig. S3B, C
 98 and D), again, no correlation was observed between CH₄ and the other biogeochemical variables, however, in the phase I and
 99 II, significant correlations are observed between the nutrients and T, S and DO (negative correlations) (Fig. S3B and C), which
 100 may be associated with the upwelling during spring-summer. In the phase III (Fig. S3D), only Si(OH)₄ showed significant

101 correlations with T (negative correlation), NO_3^- (positive correlation), PO_4^{3-} (positive correlation) and the Si:N ratio (positive
102 correlation), this may be due to Si input during the rainfall period presented in the autumn-winter period. Moreover, the slight
103 correlation (but no significant) between CH_4 and Chl-a in Phase III, suggests the possibly organic matter
104 degradation/consumption could impact CH_4 production and that low scale processes (order of hours or days) could mask this
105 correlation, since there is a wide range in the composition of the phytoplankton species are involved in CH_4 cycling (Klitzsch
106 et al., 2019, 2023; Günthel et al., 2020).

107 We further explore the multivariate relationship between CH_4 variability and other variables by separating the data into the
108 surface and subsurface layers by performing a PCA (Fig. S4). Although the CH_4 vector contributes minimally to the total
109 variance in the dataset, distinct behaviour is observed in both layers (Fig. S4A and B). In the surface layer, Principal Component
110 1 (PC1) shows almost no variability in CH_4 and accounts for 25% of the total variance. PC2 contains 22.1% of the total
111 variance and reveals a direct relationship between CH_4 and the variables Chl-a, primary production, Si:N ratio, $\text{Si}(\text{OH})_4$, PO_4^{3-} ,
112 and NO_3^- , while being negatively correlated with temperature, DO, NO_2^- , and N:P ratio. When separating dataset into phases,
113 there are differences in variability and the components (Fig. S4C and D). Surface variability is highest in Phase I and lowest
114 in Phase III. Phases I and II vary on both axes, while Phase III is mainly contained on PC2 (Fig. S4C). For the subsurface, the
115 variability is similar in all phases, but the components on which the variability occurs are more differentiated. Phase III varies
116 almost exclusively in the first dimension (the point cloud aligns along the x-axis), while Phases I and II vary on both dimensions
117 (the point cloud is oblique to the axes) (Fig. S4D), this may be due to the differentiation between the upwelling (Phases I and
118 II) and non-upwelling (Phase III) periods.

119 So, the complexity inherent in CH_4 dynamics within the study area poses a challenge to comprehension. Consequently, both
120 short- and long-term CH_4 cycling experiments have been conducted to enhance our understanding. These experiments
121 specifically target size-fractionated planktonic communities combined with organic substrates. The objective is to unravel the
122 intricate interactions and substrates that potentially influence CH_4 production. By focusing on size fractions within planktonic
123 communities, it is possible to assess the contribution of diverse groups to CH_4 production.

124 3.2 Short-term CH_4 cycling within size fractionated planktonic communities.

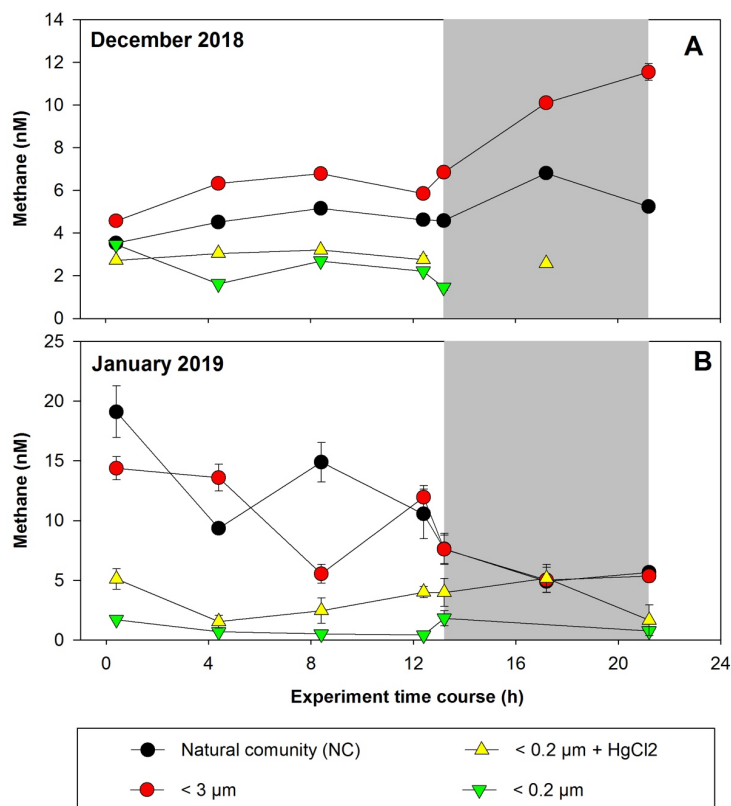
125 Figure 4 shows CH_4 accumulation/depletion in plankton-fractionated experiments over a timeframe, with daily incubations
126 (12 hours of light and 12 hours of darkness). Initial experiments were conducted in December 2018 (Fig. 4A) and January
127 2019 (Fig. 4B), corresponding to a period of high productivity or Phase I (Table S1) and coinciding with strong vertical
128 advection. The surface water exhibits cooling (~12-13 °C) and elevated CH_4 levels (9.44–17.09 nM), indicative of an active
129 upwelling period (Farias et al., 2021), aligning with other indicators of coastal upwelling (Aguirre et al., 2021).

Deleted: S3

Deleted: S3

Deleted: .

Deleted: .



134
 135 **Figure 4.** Time courses of dissolved methane concentration (nM) during incubations with fractionated plankton experiments (NC:
 136 natural community; <3 μm: picoplankton and controls (<0.2 μm). A. December 2018 and B. January 2019. Photoperiod is
 137 represented in white (light) and gray (dark). Error bars represent standard deviation of triplicate samples, when error bars are not
 138 visible, they are within the area of the symbol.

139 In the treatments involving fractions <0.2 μm and <0.2 μm + HgCl₂, which serve as negative controls, CH₄ concentrations
 140 remain relatively constant during incubation, with concentrations below 2.32 nM (Fig. 4A) and 5.51 nM (Fig. 4B), indicating
 141 biological CH₄ production (Table S2). However, abiotic CH₄ production via photooxidation of CDOM may occur (Li et al.,
 142 2020; Zhang and Xie, 2015), but this is not considered in this study. Processes such as DOM photochemical reactions (Mopper

143 et al., 2015), which can contribute to the DOM pool at shallower depths (<10 m) and be photo-oxidized to produce CH₄, are
144 disregarded under natural conditions (Li et al., 2020; Zhang and Xie, 2015). In December, CH₄ concentrations in the NC
145 (positive control) and <3 μm fractions undergo slight increases under light conditions (Fig. 4A, Table S2). However, during
146 darkness, the net CH₄ accumulation is significantly higher in the <3 μm fraction (p = 0.03; Table S2). Picoplankton includes
147 autotrophic and heterotrophic unicellular organisms in the size range of 0.2 to 2 μm. The autotrophic organisms comprise of
148 cyanobacteria (*Prochlorococcus* and *Synechococcus*) and diverse picoeukaryotes larger than 1 μm (Worden, 2006), while the
149 heterotrophic organisms are primarily prokaryotes, with bacteria overwhelmingly dominating over archaea in the upper layers
150 (Smith et al., 2013). This fraction (<3 μm) includes several coexisting metabolic groups that depend on different energy sources
151 such as sunlight, DOC, or even a combination of the two (mixotrophy). These groups are critical for the functioning of the
152 microbial food web and are predominantly responsible for DOC cycling (Muñoz-Marin et al., 2020; Reintjes et al., 2020) and
153 its derivative compounds (including CH₄).

154 In January, the experiments show distinct results, with CH₄ levels decreasing over incubation time in both the NC and <3 μm
155 fractions for both photoperiods (Fig. 4B), although the rate of consumption is lower in darkness (Table S2). These differences
156 suggest that the composition of the microbial community during the high productivity period, as well as the quantity and
157 quality of DOC and nutrient concentrations and their ratios (Allen et al., 2012; Spilling et al., 2019), control CH₄ cycling.
158 Indeed, the environmental conditions differ during sampling (Table S1); although both months are oxygenated, both vary in
159 Chl-a and nutrient levels, including CH₄ (Fig. 3C; Table S1).

160 Significant differences in CH₄ accumulation rates between the NC and <150 μm fraction treatments (data not shown) are
161 observed compared with the <3 μm fraction (Table S2). Peak cycling rates occur in the <3 μm fraction, indicating that larger
162 microorganisms do not affect the net CH₄ accumulation/consumption (Table S2), highlighting the importance of the microbial
163 loop in CH₄ cycling. Additionally, the observed differences between photoperiods in both fractions may suggest coupling
164 mechanisms between autotrophic phytoplankton and heterotrophic bacterioplankton communities (León-Palmero et al., 2020;
165 Morán et al., 2002; Repeta et al., 2016).

166 CH₄ consumption by methanotrophs should be considered in CH₄ cycling experiments, as aerobic CH₄ oxidation significantly
167 reduces the net CH₄ accumulation rates (net production vs. consumption) (Mao et al., 2022). While the impact of light on
168 methanotrophs is not widely understood (Broman et al., 2023), existing literature suggests that methanotrophs may experience
169 inhibition under light conditions (Dumestre et al., 1999; Morana et al., 2020). Consequently, CH₄ accumulation should be
170 higher under these conditions. However, this does not agree with our results (for light/dark conditions), indicating that
171 methylophs are more dynamic and complex than expected, making them difficult to understand through the observation of
172 their daily cycles.

173 3.3 Short-term CH₄ cycling experiment from picoplankton amended with organic substrates.

174 As the picoplankton fraction showed the highest rate of CH₄ accumulation (Fig. 4), this prompts its selection for assessing its
175 potential for methylotrophic methanogenesis through the addition of methylated substrates (MPn and TMA) in a daily cycle.

176 Phosphonate (MPn) and methylamines compounds (mono, di and trimethylamines) are dissolved methylated compounds
177 known to stimulate CH₄ production because they have a methyl radical (-CH₃), a potential precursor for CH₄ formation in
178 oxygenated environments (Karl et al., 2008; Repeta et al., 2016; Wang et al., 2021; Bižić-Ionescu et al., 2018).
179 These compounds are ubiquitous in various ecosystems (Lohrer et al., 2020; Sun et al., 2019), yet they have distinct metabolic
180 origins. The MPn originates from microorganisms as *Archaea Nitrosopumilus maritimus* (Metcalf et al., 2012) and *Candidatus*
181 *pelagibacter spp.* (Born et al., 2017), two of the most abundant marine microorganisms. MPn₁ is found at very low
182 concentrations (~0.01 μM, close to its analytical detection limit) likely due to rapid microbial turnover (Karl et al., 2008;
183 Martínez et al., 2013; Urata et al., 2022). The methylamines compounds as the trimethylamine compounds exhibit a wide
184 concentration range in the ocean, from nM levels in the open ocean to μM levels in sediments and near the coast (Sun et al.,
185 2019). Environmental TMA concentrations could be higher, particularly in upwelling regions that bring the TMA from bottom
186 waters to the surface (Gibb et al., 1999; Sun et al., 2019). In this context, the amendments performed for each substrate, 100-
187 fold for MPn and 1000-fold for TMA, convert these experiments into potential rates.
188 These amendment experiments were conducted in Phase II (March 2019) and Phase III (May 2019), periods of change in
189 phytoplankton succession (composition), biomass and abundance (Testa et al., 2018). In winter, the relative abundance of
190 picoplankton with respect to microplankton (particularly the presence of *Synechococcus* and nitrifying archaea) increases
191 significantly, especially photosynthetic picoeukaryotes (Collado-Fabbi et al., 2011). The time course CH₄ accumulation
192 during incubations is illustrated in Fig. 5. ~~We observe highly variable temporal fluctuations during these periods (March and~~
193 ~~May). A particularity is the is the abrupt increase in CH₄ concentration upon transitioning from light to dark cycles in March~~
194 ~~(Phase II), as well as the significant CH₄ accumulation that persists in darkness (Fig. 5A). In May (Phase III), the time course~~
195 ~~distribution of CH₄ in each treatment exhibits considerable variability. Notably, the addition of MPn results in greater~~
196 ~~accumulation in CH₄, particularly in darkness, accompanied by a pronounced increase over incubation time (Fig. 5B; Table~~
197 ~~S2). In both periods, the <3 μm + MPn treatment exhibits contrasting patterns under dark conditions (Fig. 5A and 4B),~~
198 ~~decreasing in Phase II, and increasing in Phase III, suggesting the importance of microbial composition. During winter, (Phase~~
199 ~~III), a higher DOC concentration is found (Fig 3E), which may lead to higher bacterial and archaeal activity that could be~~
200 ~~metabolizing DOC, including MPn under dark conditions. On the other hand, despite a coefficient of variation <10%, we~~
201 ~~cannot entirely discount experimental issues in the abrupt rise of the <3 μm + MPn treatment at around 12 hours.~~

Deleted: Arquea

Formatted: Font color: Black

Deleted: The highest CH₄ accumulation are observed in the MPn-amended treatment, particularly under dark conditions in May (Phase III) (Fig. 5B; Table S1). Interestingly, in

Deleted: and

Deleted: ,

Deleted: observed

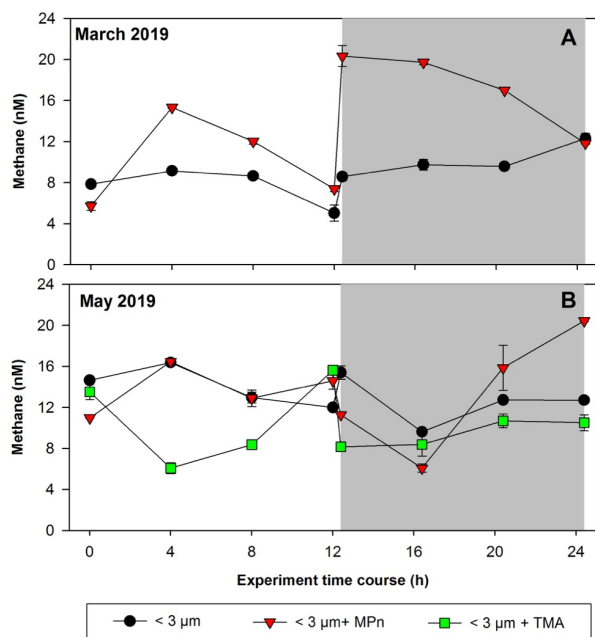


Figure 5. Time courses of dissolved methane concentration (nM) during incubations with the addition of methylated substrates (MPn: methyl phosphonic acid and TMA: trimethylamine) performed with bacterioplankton (<3 μm) and bacterioplankton concentrate (CC). A. March 2019 and B. May 2019. Photoperiod is represented in white (light) and gray (dark). Error bars represent standard deviation of triplicate samples, when error bars are not visible, they are within the area of the symbol.

Conversely, the TMA treatment does not result in any CH₄ accumulation, being lower compared to the control and MPn treatments (Fig. 5B); while TMA can be metabolized by marine bacteria (Lidbury et al., 2015; Bižić-Ionescu et al., 2018), the reduced CH₄ production in this treatment suggests an end product different than CH₄ (Sun et al., 2019). In contrast, heterotrophic picoplankton might metabolize MPn and produce CH₄, showing *in situ* methanogenesis via the carbon-phosphorus (C-P) lyase pathway (Karl et al., 2008).

3.4 Long-term CH₄ cycling from concentrated picoplankton amended with organic substrates.

For a more comprehensive understanding, our study involves long-term microcosm experiments conducted during two distinct phases of productivity. One of these phases occurs during intermediate productivity (Phase II or late summer to autumn),

Deleted: lower

Deleted: a

Deleted: outcome

i25 characterized by a notable prevalence of autotrophic small diatoms, pico-eukaryotes, and cyanobacteria (*Synechococcus*), in
i26 contrast to the high productivity period (Phase I or early springtime) (Fig. S5A and D), where large diatoms are predominant
i27 (Fig. S5B and E), while heterotrophic bacterioplankton exhibits an almost constant presence in both periods (Fig. S5C and F).
i28 These temporal distributions align with well-documented phytoplankton and bacterioplankton patterns in our study area
i29 (Aldunate et al., 2018; Collado-Fabbri et al., 2011; De La Iglesia et al., 2020; Molina et al., 2020).

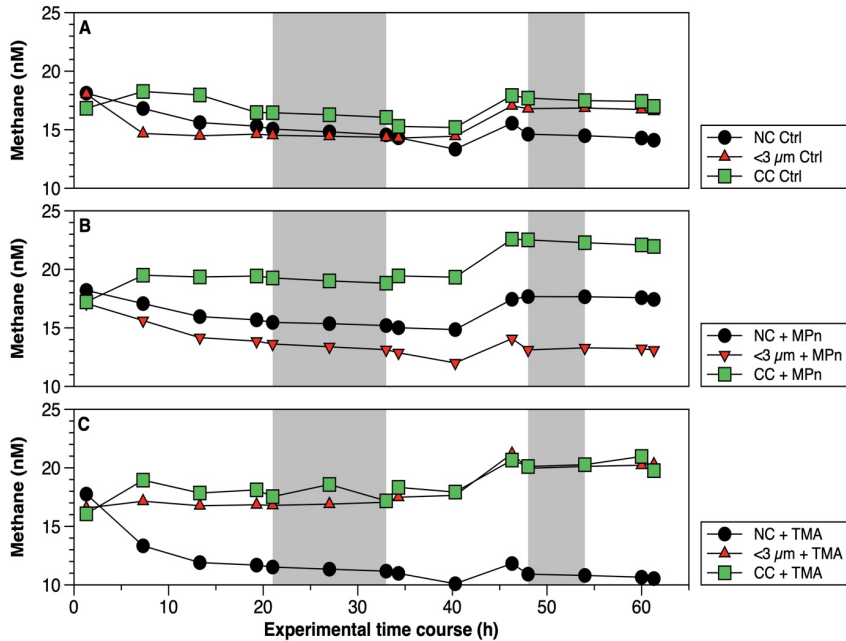
i30 Briefly, Flavobacteraceae, SAR11 subclade IA (*Candidatus Pelagibacter spp.*), SAR11 subclade 1b, gammaproteobacterial
i31 clades, and SAR86 are prevalent during upwelling seasons, while during non-upwelling seasons or Phase III, SAR11 subclade
i32 II, Marine Actinobacteria, and unclassified Alphaproteobacteria dominate (Aldunate et al., 2018). In addition, photosynthetic
i33 picoplankton eukaryotes related to Mamiellophyceae (*Bathycoccus*, *Micromonas*, and *Ostreococcus*) are predominantly
i34 observed with high significance in the surface layer during the transition period (Collado-Fabbri et al., 2011; De La Iglesia et
i35 al., 2020), whereas the abundance of heterotrophic bacteria, ranging from 0.23 to 6.50 x10⁶ cells mL⁻¹, is mainly concentrated
i36 in the surface during late summer and autumn, with minima in winter (Molina et al., 2020). However, in our study, the
i37 abundance of heterotrophic bacteria shows no significant differences (p = 0.05) in both periods (1 x 10⁶ cells mL⁻¹) (Fig. S5C
i38 and F). This is due to the low DOC at the beginning of the upwelling period (Fig. 3E).

i39 The CH₄ accumulations during time incubations under different treatments in Phase II are illustrated in Figure 6. Net CH₄
i40 cycling rates are detailed in Table S4. Variations are observed when these rates are differentiated between light and dark
i41 periods, as well as across different periods or phases of productivity (Table S4). The concentrated community (CC) results in
i42 substantial enrichments of cyanobacteria (*Synechococcus*), picoeukaryotes, and heterotrophic bacteria by factors of 1.9, 1.8,
i43 and 4.6, respectively, compared to the NC, and factors of 1.8, 1.8, and 6.1, respectively, in relation to the natural <3 μm
i44 fraction (Figure S5A, B, and C). In both cases, a significant increase in bacteria is observed (Figure S5C). The microbial
i45 abundance proportions in the NC treatment at the beginning of the experiment closely align with field observations (Collado-
i46 Fabbri et al., 2011; Anabalón et al., 2007; Morales et al., 2007).

i47

Deleted: *ubique-associated*),

Formatted: Left



i49
i50 **Figure 6.** Time courses of dissolved methane (nM) during incubation in long-term microcosm experiments (10L) with the addition
i51 of methylated substrates (MPn: methyl phosphonic acid and TMA: trimethylamine) performed with three planktonic communities
i52 (NC: natural community; <3 μm: bacterioplankton and CC: community concentrate) under oxygenated conditions in April 2019.
i53 Photoperiod is represented in white (light) and gray (dark).

i54 Mean Chl-a levels in the <3 μm fraction are 21.7 and 4.5 times lower than in the NC and CC, respectively (Table S3). This
i55 suggests that this fraction contains phyto-picoeukaryotes (e.g., coccolithophorids, cryptophytes) and picocyanobacteria (e.g.,
i56 *Synechococcus*) in a lower proportion than the CC. Additionally, the CC treatment displays higher background levels of DOC
i57 and nutrients probably due to the natural diurnal mortality of picoplankton (Llabrés et al., 2011). It cannot be ruled out that the
i58 baseline is due to tangential flow filtration, although it is one of the most used methods to concentrate DOM (Benner et al.,
i59 1992), reducing the amount of membrane sorption and fouling (Minor et al., 2014).

i60 In April (Phase II), CH₄ cycling rates consistently exhibit higher values during the dark phase, suggesting a significant
i61 involvement of heterotrophic bacterioplankton (Table S4). Additionally, these rates are notably elevated in the CC treatments,
i62 particularly in the CC + MPn (Table S4). When comparing the treatments (NC, <3 μm, and CC) without (controls) and with
i63 the addition of MPn and TMA (Fig. 6, Table S4), although temporal patterns are similar, significant differences between

Formatted: Font color: Auto, Ligatures: None

64 treatments ($p = 0.002$) are found with slightly higher CH₄ cycling rates in <3 μm in dark conditions (Fig. 6A; Table S4). With
 65 the addition of MPn (Fig. 6B; Table S4), the CC + MPn treatment, characterized by the highest abundance of autotrophic
 66 (cyanobacteria) and heterotrophic microorganisms (Fig. S5), exhibits a significant increase in a net CH₄ accumulation, in both
 67 light and dark conditions (Table S4). In addition, higher Chl-a concentrations (Table S3) in the NC treatment may have
 68 supported greater CH₄ accumulation compared to the <3 μm fraction (Fig. 6B). Regarding the TMA enrichment (Fig. 6C),
 69 both the CC and the <3 μm fraction treatments respond similarly, increasing CH₄ concentration over time ($p = 3 \times 10^{-6}$; Fig. 6C)
 70 although the recycling rates were slightly higher in <3 μm + TMA, suggesting that microbial abundance does not significantly
 71 affect CH₄ production with TMA or that the heterotrophic community in the CC treatment weakly metabolizes TMA (De
 72 Angelis and Lee, 1994; Bižić-Ionescu et al., 2018).
 73 Although the metabolism of methylated substrates, such as MPn to CH₄ by various types of bacteria, has been extensively
 74 documented (Repeta et al., 2016; Del Valle and Karl, 2014; Metcalf et al., 2012; Zhao et al., 2022; Damm et al., 2010; Karl et
 75 al., 2008), this has only been reported mostly under phosphorus-starved conditions. However, this is unlikely in our study area,
 76 which experienced high PO₄³⁻ availability, even in excess compared to N (Table 2). Specifically, the expression of phosphonate
 77 C-P lyase genes could arise when P-starved (Carini et al., 2014; Taenzer, 2019; Sosa et al., 2019). Thus, an alternative
 78 explanation for the significant CH₄ accumulation in the CC with MPn treatment could be related to the presence of
 79 photosynthetic cyanobacteria (Bižić et al., 2020), which have adaptive strategies to fluctuating P levels (Li and Ditttrich, 2019).
 80 This is further complemented by the capacity of some bacteria to degrade phosphonates in environments with a substantial
 81 background of P (Schowanek and Verstraete, 1990).
 82 Given that *Synechococcus* dominates during the non-upwelling period (autumn-winter season) in the photic layer (Collado-
 83 Fabbri et al., 2011), it becomes plausible to consider CH₄ production mediated by this microorganism in this period.
 84 Consequently, CH₄ production pathways appear multifaceted, involving complex interplays between photochemical and
 85 metabolic processes. The mechanism by which cyanobacteria effectively convert fixed CO₂ to CH₄ under light conditions
 86 appears intricately linked to the photosynthetic process (Bižić et al., 2020; Klintzsch et al., 2020) as inhibitors of photosynthesis
 87 blocked CH₄ production under light conditions (Bižić et al., 2020). They suggest that distinct mechanisms might govern CH₄
 88 production under light and dark conditions, influenced by freshly synthesized photosynthetic products in light and storage
 89 compounds during darkness.
 90 In September (Phase I), CH₄ cycling rates exhibit substantial differences compared to those estimated for Phase II. Notably,
 91 these rates are lower in most treatments, with a reversal observed in the pattern compared to Phase II, i.e., CH₄ cycling rates
 92 during light condition surpass those during dark condition (Table S4). Furthermore, the CC treatments consistently demonstrate
 93 the highest rates compared to the other treatments (Table S4). Temporal CH₄ accumulation in this phase, consistently
 94 demonstrates higher CH₄ levels in the CC treatment compared to the NC and <3 μm fraction (controls) (Fig. 7A). However, a
 95 noteworthy contrast appears when considering the impact of substrate additions. Specifically, the addition of TMA in the CC
 96 treatment in this phase results in a more pronounced CH₄ production (Fig. 7C) compared to the effect of MPn (Fig. 7B),
 97 especially in dark conditions (Table S4). This pattern, the opposite of that found in Phase II, could potentially be explained by

Deleted: accumulation during the second photoperiod, especially

Deleted: the CC and

Deleted: fractions

Deleted:). This suggests that during the first photoperiod, there may be changes and/or acclimation of planktonic communities.

Deleted: +

Deleted: .

Deleted: 6C) and

Formatted: Ligatures: None

Formatted: Font color: Black, Ligatures: Standard + Contextual

Deleted: our upwelling system.

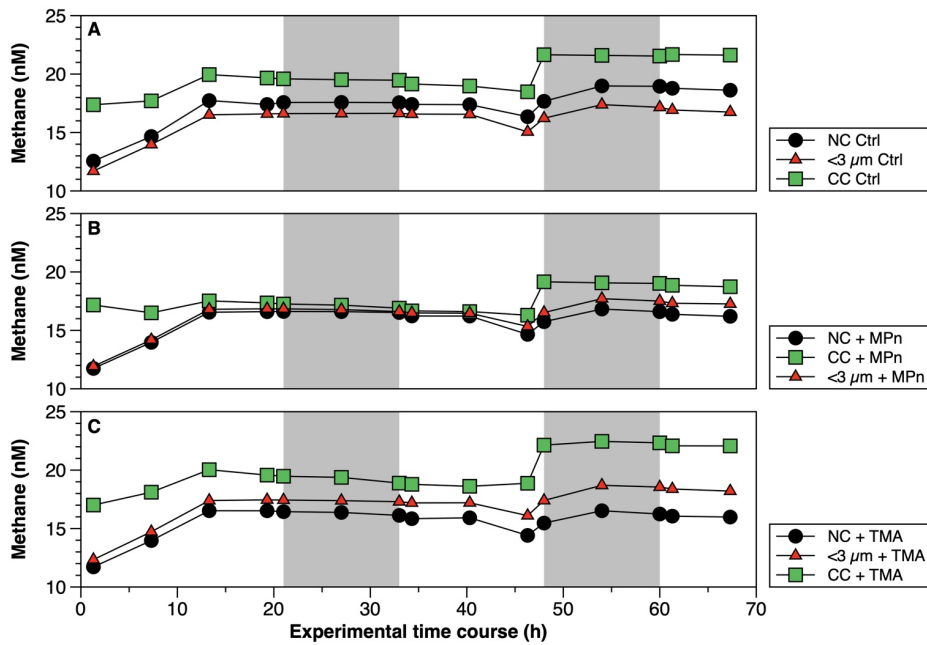
Deleted: During Phase I, temporal CH₄ accumulation

Deleted: introduction

Deleted: 7B).

i10 the observed decrease in *Synechococcus* abundance (Fig. S5D), which remains unresponsive to MPn, and the concurrent
i11 increase in nano and picoeukaryotes and bacteria at the end of the experiment (Fig. S5E and F); the last of which ~~could be~~
i12 conducive to the action of TMA (Bižić-Ionescu et al., 2018; De Angelis and Lee, 1994; Lidbury et al., 2015). Indeed, a marked
i13 reduction in *Synechococcus* abundance is observed (showing a 4.6-fold decrease) compared to the Phase II (Fig. S5A and D),
i14 whereas nano- and picoeukaryotes experience notable abundance (3.1 to 3.7 times higher than the transition period) (Fig. S5B
i15 and E).
i16

Deleted: is

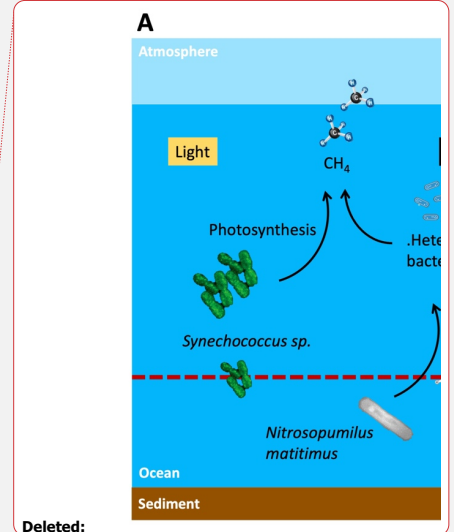
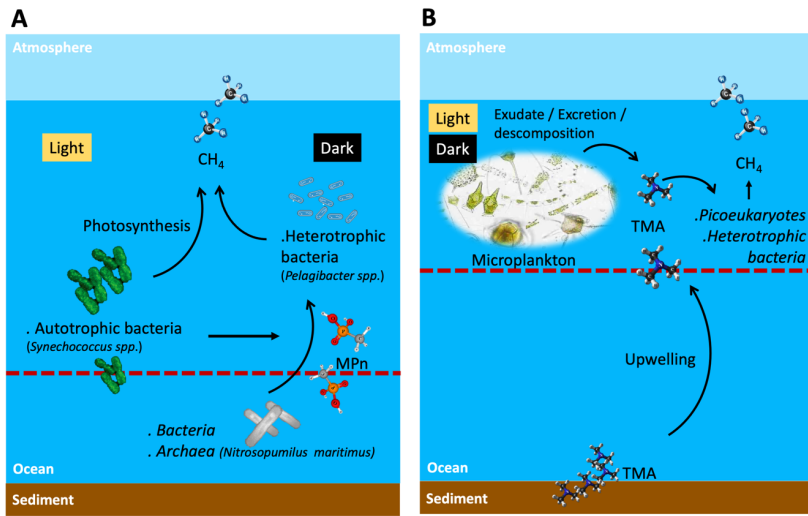


i17
i18 **Figure 7.** Time courses of dissolved methane (nM) during incubation in long-term microcosm experiments (10L) with the addition
i19 of methylated substrates (MPn: methyl phosphonic acid and TMA: trimethylamine) performed with three planktonic communities
i20 (NC: natural community; <3 μm: bacterioplankton and CC: community concentrate) under oxygenated conditions in September
i21 2019. Photoperiod is represented in white (light) and gray (dark).

i22 In this phase, the distribution proportions within the NC treatment are cyanobacteria, nano and picoeukaryotes, and bacteria
i23 accounted for 1.1, 2.3 and 96.6, respectively. In contrast, within the CC treatment, the initial distribution proportions are higher
i24 with respect to the NC: cyanobacteria, picoeukaryotes, and bacterioplankton displayed proportions 1.6, 0.6, and 2.9 times

Deleted: (1),

i27 greater, respectively. This underscores the increased significance of bacteria and autotrophic picoeukaryotes during this phase,
i28 as further corroborated by Chl-a measurements (Table S3). An intricate interplay between microbial communities and CH₄
i29 cycling within distinct phases of productivity is schematically illustrate in Figure 8. The prevalence of cyanobacteria,
i30 picoeukaryotes, and heterotrophic bacteria varied significantly between these phases. So, this indicates that substrate utilization
i31 is related to the availability of nutrients as well as the complexity of the substrate and the composition of the heterotrophic
i32 bacterial community, potentially driving CH₄ production dynamics.
i33



i34
i35 **Figure 8. Suggested scheme of methane cycling mechanisms in two contrasting periods of primary production and oceanographic**
i36 **conditions during light and dark phases, where potential planktonic communities and methylated substrates are involved to**
i37 **metabolize methane in surface waters. A. Phase II and III or late upwelling or non-upwelling season and B. Phase I or active**
i38 **upwelling season. Dashed line shows the 100 μmol L⁻¹ oxycline, above this line oxalic methane is produced. TMA: trimethylamine;**
i39 **and MPn: methyl phosphonic acid.**

i40 High CH₄ levels in surface water during the non-upwelling period, comparable to the upwelling period, could result from in
i41 situ CH₄ production mediated by photosynthetic *Synechococcus* or demethylation by heterotrophic bacteria (Fig. 8A). On the
i42 other hand, although the trimethylamine methyltransferase enzyme has been described as involved in the demethylation of
i43 TMA in methanogen microorganisms (Paul et al., 2000), it cannot be ruled out that in Phase I (spring) heterotrophic bacteria
i44 dominance can metabolize TMA through an alternative pathway still unknown (Fig. 8B), nor can it be ruled out that the
i45 upwelling brings methanogens with the necessary machinery to metabolize TMA at the ocean surface.

47 4 Conclusions

48 Overall, picoplankton produced CH₄ in all experiments conducted in both light and dark conditions, although the net CH₄
49 production rate was higher in dark conditions. Moreover, laboratory experiments demonstrated that organic compounds such
50 as TMA and MPn are metabolized by heterotrophic bacterioplankton, contributing to the production of oxic CH₄ in the
51 oxygenated surface layer.

52 Coastal upwelling could bring with it organic amino compounds such as TMA including mono and di trimethylamines from
53 sediments, which added to plankton decomposition compounds, and change in picoplanktonic composition (bacteria and the
54 remarkable increase of pico- and nano eukaryotes) during the favorable upwelling period, could promote CH₄ production via
55 TMA, through a pathway that is still unknown, but would potentially add to CH₄ supersaturation in the oxygenated surface
56 layer, beyond the contribution of CH₄ by advection.

57 *Synechococcus* could be responsible for CH₄ regeneration through photosynthesis. These cyanobacteria are abundant in the
58 non-upwelling period, and together with other picoeukaryotes, maintain intermediate and basal Chl-a levels during this period
59 that matched with higher DOC levels and inorganic N:P ratios (compared to the upwelling period). This may stimulate
60 heterotrophic bacteria to metabolize MPn and thus contribute to the recycling of oxic CH₄.

61 It is important to note that amended experiments were conducted in Phase II (March 2019) and Phase III (May 2019), periods
62 marked by changes in the phytoplankton succession (composition), biomass and abundance in winter, the relative abundance
63 of picoplankton with respect to microplankton (particularly the presence of *Synechococcus* and *nitrifying archaea*) increases
64 significantly, especially photosynthetic picoeukaryotes.

65 **Acknowledgements** Thanks to Gerardo Garcia for his experience and teaching in the use of laboratory equipment and his help
66 in setting up the experiments; and Karen Sanzana for nutrient analysis; Oliver Alarcon for oxygen analysis. Both the crew of
67 R/V Kay Kay (II) and the Dichato Marine Station of the University of Concepcion provided valuable help during fieldwork,
68 as well as all participating colleagues in the time series station (University of Concepcion), who provided the core
69 measurements. We also appreciate the work done during the COVID pandemic by Juan Faúndez. This research was funded
70 by the Fondo Nacional de Investigaciones Científicas y Tecnológicas (FONDECYT) grant N° 1200861 and also
71 Millennium Science Initiative Program ICM 2019-015 (SECOS) and CR2 FONDAP-CONICYT N° 1522A001.

72

i73 **References**

- i74 Aguirre, C., Pizarro, Ó., Strub, P. T., Garreaud, R., and Barth, J. A.: Seasonal dynamics of the near-surface alongshore flow
i75 off central Chile, *J Geophys Res Oceans*, 117, <https://doi.org/10.1029/2011JC007379>, 2012.
- i76 Aguirre, C., Garreaud, R., Belmar, L., Fariás, L., Ramajo, L., and Barrera, F.: High-frequency variability of the surface ocean
i77 properties off central Chile during the upwelling season, *Front Mar Sci*, 8, 1–19, <https://doi.org/10.3389/fmars.2021.702051>,
i78 2021.
- i79 Aldunate, M., De la Iglesia, R., Bertagnolli, A. D., and Ulloa, O.: Oxygen modulates bacterial community composition in the
i80 coastal upwelling waters off central Chile, *Deep Sea Research Part II Topical Studies in Oceanography*, 156, 68–79,
i81 <https://doi.org/10.1016/j.dsr2.2018.02.001>, 2018.
- i82 Allen, L. Z., Allen, E. E., Badger, J. H., McCrow, J. P., Paulsen, I. T., Elbourne, L. D., Thiagarajan, M., Rusch, D. B., Nealson,
i83 K. H., Williamson, S. J., Venter, J. C., and Allen, A. E.: Influence of nutrients and currents on the genomic composition of
i84 microbes across an upwelling mosaic, *ISME Journal*, 6, 1403–1414, <https://doi.org/10.1038/ismej.2011.201>, 2012.
- i85 Anabalón, V., Morales, C. E., Escribano, R., Varas, A. M., and Varas, M. A.: The contribution of nano- and micro-planktonic
i86 assemblages in the surface layer (0–30 m) under different hydrographic conditions in the upwelling area off Concepción,
i87 central Chile, *Prog Oceanogr*, 75, 396–414, <https://doi.org/10.1016/j.pocean.2007.08.023>, 2007.
- i88 De Angelis, M. A. and Lee, C.: Methane production during zooplankton grazing on marine phytoplankton, *Limnol. Oceanogr.*,
i89 39, 1298–1308, 1994.
- i90 Bange, H. W., Bartell, U. H., Rapsomanikis, S., and Andreae, M. O.: Methane in the Baltic and North Seas and a reassessment
i91 of the marine emissions of methane, *Global Biogeochem Cycles*, 8, 465–480, 1994.
- i92 Bauer, J. and Druffel, E.: Ocean margins as a significant source of organic matter to the deep open ocean, *Letter to nature*,
i93 392, 482–485, <https://doi.org/https://doi.org/10.1038/33122>, 1998.
- i94 Bello, E.: Variabilidad estacional en la descarga de metano disuelto desde un sistema estuarino a la zona marina adyacente, el
i95 caso de ríos de la zona central de Chile (río Itata), Universidad de Concepción, 76 pp., 2016.
- i96 Belviso, S., Kim, S. -K., Rassoulzadegan, F., Krajka, B., Nguyen, B. C., Mihalopoulos, N., and Buat-Menard, P.: Production
i97 of dimethylsulfonium propionate (DMSP) and dimethylsulfide (DMS) by a microbial food web, *Limnol Oceanogr*, 35, 1810–
i98 1821, <https://doi.org/10.4319/lo.1990.35.8.1810>, 1990.
- i99 Benner, R., Dean Pakulski, J., Mccarthy, M., Hedges, J. I., Hatcher, P. G., Benner, R., Pakulski, J. D., McCarthy, M., Hedges,
'00 J. I., Hatcher, P. G., H van Beest, B. W., Kramer, G. J., and van Santen, R. A.: Bulk chemical characteristics of dissolved
'01 organic matter in the ocean, *J. Glinnemann, ibid*, 255, 1561–1564, <https://doi.org/DOI:10.1126/science.255.5051.1561>, 1992.
- '02 Berg, A., Lindblad, P., and Svensson, B. H.: Cyanobacteria as a source of hydrogen for methane formation, *World J Microbiol*
'03 *Biotechnol*, 30, 539–545, <https://doi.org/10.1007/s11274-013-1463-5>, 2014.
- '04 Bianchi, T. S.: The role of terrestrially derived organic carbon in the coastal ocean: A changing paradigm and the priming
'05 effect, <https://doi.org/10.1073/pnas.1017982108>, 6 December 2011.

'06 Bizic, M.: Phytoplankton photosynthesis: An unexplored source of biogenic methane emission from oxic environments, *J*
'07 *Plankton Res*, 43, 822–830, <https://doi.org/10.1093/plankt/fbab069>, 2021.

'08 Bižić, M., Klintzsch, T., Ionescu, D., Hindiyeh, M. Y., Günthel, M., Muro-Pastor, A. M., Eckert, W., Urich, T., Keppler, F.,
'09 and Grossart, H. P.: Aquatic and terrestrial cyanobacteria produce methane, *Sci Adv*, 6, 1–10,
'10 <https://doi.org/10.1126/sciadv.aax5343>, 2020.

'11 Bižić-Ionescu, M., Ionescu, D., Günthel, M., Tang, K. W., and Grossart, H. P.: Oxic methane cycling: new evidence for
'12 methane formation in oxic lake water, *Biogenesis of Hydrocarbons*, 1–22, <https://doi.org/10.1007/978-3-319-53114-4>, 2018.

'13 Borges, A. V. and Abril, G.: Carbon Dioxide and Methane Dynamics in Estuaries, Elsevier Inc., 119–161 pp.,
'14 <https://doi.org/10.1016/B978-0-12-374711-2.00504-0>, 2012.

'15 [Born, D. A., Ulrich, E. C., Ju, K. S., Peck, S. C., Van Der Donk, W. A., and Drennan, C. L.: Structural basis for](https://doi.org/10.1126/science.aao3435)
'16 [methylphosphonate biosynthesis, *Science* \(1979\), 358, 1336–1339, https://doi.org/10.1126/science.aao3435, 2017.](https://doi.org/10.1126/science.aao3435)

'17 Broecker, W. S. and Peng, T. H.: Gas exchange rates between air and sea, *Tellus XXVI*, 1, 21–35,
'18 <https://doi.org/10.1111/j.2153-3490.1974.tb01640.x>, 1974.

'19 Broman, E., Barua, R., Donald, D., Roth, F., Humborg, C., Norkko, A., Jilbert, T., Bonaglia, S., and Nascimento, F. J. A.: No
'20 evidence of light inhibition on aerobic methanotrophs in coastal sediments using eDNA and eRNA, *Environmental DNA*, 5,
'21 766–781, <https://doi.org/10.1002/edn3.441>, 2023.

'22 Brown, I. J., Torres, R., and Rees, A. P.: The origin of sub-surface source waters define the sea-air flux of methane in the
'23 Mauritanian Upwelling, NW Africa, *Dynamics of Atmospheres and Oceans*, 67, 39–46,
'24 <https://doi.org/10.1016/j.dynatmoce.2014.06.001>, 2014.

'25 Bullister, J. L., Wisegarver, D. P., and Wilson, S. T.: The production of methane and nitrous oxide gas standards for Scientific
'26 Committee on Ocean Research (SCOR) Working Group #143, 1–9 pp., 2016.

'27 Capelle, D. W. and Tortell, P. D.: Factors controlling methane and nitrous-oxide variability in the southern British Columbia
'28 coastal upwelling system, *Mar Chem*, 179, 56–67, <https://doi.org/10.1016/j.marchem.2016.01.011>, 2016.

'29 Capone, D. G. and Hutchins, D. A.: Microbial biogeochemistry of coastal upwelling regimes in a changing ocean,
'30 <https://doi.org/10.1038/ngeo1916>, September 2013.

'31 Carini, P., White, A. E., Campbell, E. O., and Giovannoni, S. J.: Methane production by phosphate-starved SAR11
'32 chemoheterotrophic marine bacteria, *Nat Commun*, 5, 1–7, <https://doi.org/10.1038/ncomms5346>, 2014.

'33 Carpenter, J.: Do rats and pigeons readily acquire instrumental responses for food in the presence of free food?, *Limnol*
'34 *Oceanogr*, 10, 141–143, <https://doi.org/10.3758/BF03209628>, 1965.

'35 Carpenter, L. J., Archer, S. D., and Beale, R.: Ocean-atmosphere trace gas exchange, *Chem Soc Rev*, 41, 6473–6506,
'36 <https://doi.org/10.1039/c2cs35121h>, 2012.

'37 Cerbin, S., Pérez, G., Rybak, M., Wejnerowski, Ł., Konowalczyk, A., Helmsing, N., Naus-Wiezer, S., Meima-Franke, M.,
'38 Pytlak, Ł., Raaijmakers, C., Nowak, W., and Bodelier, P. L. E.: Methane-derived carbon as a driver for cyanobacterial growth,
'39 *Front Microbiol*, 13, 1–16, <https://doi.org/10.3389/fmicb.2022.837198>, 2022.

'40 Cicerone, R. J. and Oremland, R. S.: Biogeochemical aspects of atmospheric methane, *Global Biogeochem Cycles*, 2, 299–
'41 327, <https://doi.org/10.1029/GB002i004p00299>, 1988.

'42 Collado-Fabbri, S., Vaultot, D., and Ulloa, O.: Structure and seasonal dynamics of the eukaryotic picophytoplankton
'43 community in a wind-driven coastal upwelling ecosystem, *Limnol. Oceanogr.*, 56, 2334–2346,
'44 <https://doi.org/10.4319/lo.2011.56.6.2334>, 2011.

'45 Cuevas, L. A., Daneri, G., Jacob, B., and Montero, P.: Microbial abundance and activity in the seasonal upwelling area off
'46 Concepción (~36°S), central Chile: A comparison of upwelling and non-upwelling conditions, *Deep Sea Res 2 Top Stud*
'47 *Oceanogr*, 51, 2427–2440, <https://doi.org/10.1016/j.dsr2.2004.07.026>, 2004.

'48 Damm, E., Helmke, E., Thoms, S., Schauer, U., Nöthig, E., Bakker, K., and Kiene, R. P.: Methane production in aerobic
'49 oligotrophic surface water in the central Arctic Ocean, *Biogeosciences*, 7, 1099–1108, [https://doi.org/10.5194/bg-6-10355-](https://doi.org/10.5194/bg-6-10355-2009)
'50 2009, 2010.

'51 Damm, E., Beszczynska-Möller, T. A., Nöthing, E. M., and Kattner, G.: Methane excess production in oxygen-rich polar water
'52 and a model of cellular conditions for this paradox, *Polar Sci*, 9, 327–334, <https://doi.org/10.1016/j.polar.2015.05.001>, 2015.

'53 Dinasquet, J., Tirola, M., and Azam, F.: Enrichment of bacterioplankton able to utilize one-carbon and methylated compounds
'54 in the Coastal Pacific Ocean, *Front Mar Sci*, 5, 1–13, <https://doi.org/10.3389/fmars.2018.00307>, 2018.

'55 Dumestre, J. F., Guézennec, J., Galy-Lacaux, C., Delmas, R., Richard, S., and Labroue, L.: Influence of light intensity on
'56 methanotrophic bacterial activity in Petit Saut Reservoir, French Guiana, *Appl Environ Microbiol*, 65, 534–539,
'57 <https://doi.org/10.1128/aem.65.2.534-539.1999>, 1999.

'58 Fariás, L., Graco, M., and Ulloa, O.: Temporal variability of nitrogen cycling in continental-shelf sediments of the upwelling
'59 ecosystem off central Chile, *Deep Sea Res 2 Top Stud Oceanogr*, 51, 2491–2505, <https://doi.org/10.1016/j.dsr2.2004.07.029>,
'60 2004.

'61 Fariás, L., Fernández, C., Faúndez, J., Cornejo, M., and Alcaman, M. E.: Chemolithoautotrophic production mediating the
'62 cycling of the greenhouse gases N_2O and CH_4 in an upwelling ecosystem, *Biogeosciences*, 6, 3053–3069,
'63 <https://doi.org/https://doi.org/10.5194/bg-6-3053-2009>, 2009.

'64 Fariás, L., Besoain, V., and García-Loyola, S.: Presence of nitrous oxide hotspots in the coastal upwelling area off central
'65 Chile: an analysis of temporal variability based on ten years of a biogeochemical time series, *Environmental Research Letters*,
'66 10, 1–13, <https://doi.org/10.1088/1748-9326/10/4/044017>, 2015.

'67 Fariás, L., Tenorio, S., Sanzana, K., and Faúndez, J.: Temporal methane variability in the water column of an area of seasonal
'68 coastal upwelling: A study based on a 12 year time series, *Prog Oceanogr*, 195, <https://doi.org/10.1016/j.pocean.2021.102589>,
'69 2021.

'70 Ferderlman, T. G., Lee, C., Pantoja, S., Harder, J., Bebout, B. M., and Fossing, H.: Sulfate reduction and methanogenesis in a
'71 Thioploca- dominates sediment off the coast of Chile, *Geochim Cosmochim Acta*, 61, 3065–3079,
'72 [https://doi.org/https://doi.org/10.1016/S0016-7037\(97\)00158-0](https://doi.org/https://doi.org/10.1016/S0016-7037(97)00158-0), 1997.

Formatted: Subscript

Formatted: Subscript

'73 Fernandez, C., González, M. L., Muñoz, C., Molina, V., and Farias, L.: Temporal and spatial variability of biological nitrogen
'74 fixation off the upwelling system of central Chile (35-38.5°S), *J Geophys Res Oceans*, 120, 3330–3349,
'75 <https://doi.org/10.1002/2014JC010410>, 2015.

'76 Florez-Leiva, L., Damm, E., Fariás, L., and Farias, L.: Methane production induced by dimethylsulfide in surface water of an
'77 upwelling ecosystem, *Prog Oceanogr*, 112–113, 38–48, <https://doi.org/10.1016/j.pocean.2013.03.005>, 2013.

'78 Gibb, S. W., Mantoura, R. F. C., Liss, P. S., and Barlow, R. G.: Distributions and biogeochemistries of methylamines and
'79 ammonium in the Arabian Sea, *Deep Sea Res 2 Top Stud Oceanogr*, 46, 593–615, <https://doi.org/10.1016/S0967->
'80 0645(98)00119-2, 1999.

'81 Giovannoni, S. J., Delong, E. F., Schmidt, T. M., and Pace, N. R.: Tangential flow filtration and preliminary phylogenetic
'82 analysis of marine picoplankton, *Appl Environ Microbiol*, 56, 2572–2575, 1990.

'83 González, H. E., Menschel, E., Aparicio, C., and Barria, C.: Spatial and temporal variability of microplankton and detritus,
'84 and their export to the shelf sediments in the upwelling area off Concepción, Chile (~36°S), during 2002-2005, *Prog Oceanogr*,
'85 75, 435–451, <https://doi.org/10.1016/j.pocean.2007.08.025>, 2007.

'86 Grasshoff, K., Ehrhardt, M., and Kremling, K.: *Methods of Seawater Analysis*. Second, Second, Re., John Wiley & Sons, Ltd,
'87 Deerfield Beach, Florida: Verlag Chemie, 419 pp., <https://doi.org/10.1002/iroh.19850700232>, 1983.

'88 Grossart, H. P., Frindte, K., Dziallas, C., Eckert, W., and Tang, K. W.: Microbial methane production in oxygenated water
'89 column of an oligotrophic lake, *Proc Natl Acad Sci U S A*, 108, 19657–19661, <https://doi.org/10.1073/pnas.1110716108>,
'90 2011.

'91 Günthel, M., Donis, D., Kirillin, G., Ionescu, D., Bizic, M., McGinnis, D. F., Grossart, H. P., and Tang, K. W.: Contribution
'92 of oxic methane production to surface methane emission in lakes and its global importance, *Nat Commun*, 10,
'93 <https://doi.org/10.1038/s41467-019-13320-0>, 2019.

'94 Günthel, M., Klawonn, I., Woodhouse, J., Bižić, M., Ionescu, D., Ganzert, L., Kümmel, S., Nijenhuis, I., Zoccarato, L.,
'95 Grossart, H. P., and Tang, K. W.: Photosynthesis-driven methane production in oxic lake water as an important contributor to
'96 methane emission, *Limnol Oceanogr*, 1–13, <https://doi.org/10.1002/lno.11557>, 2020.

'97 Hahn, M. W.: Broad diversity of viable bacteria in “sterile” (0.2 µm) filtered water, *Res Microbiol*, 155, 688–691,
'98 <https://doi.org/10.1016/j.resmic.2004.05.003>, 2004.

'99 Hansell, D. A. and Orellana, M. V.: Dissolved organic matter in the global ocean: A primer,
'00 <https://doi.org/10.3390/gels7030128>, 1 September 2021.

'01 Harmsen, M., van Vuuren, D. P., Bodirsky, B. L., Chateau, J., Durand-Lasserve, O., Drouet, L., Fricko, O., Fujimori, S.,
'02 Gernaat, D. E. H. J., Hanaoka, T., Hilaire, J., Keramidas, K., Luderer, G., Moura, M. C. P., Sano, F., Smith, S. J., and Wada,
'03 K.: The role of methane in future climate strategies: mitigation potentials and climate impacts, *Clim Change*, 163, 1409–1425,
'04 <https://doi.org/10.1007/s10584-019-02437-2>, 2020.

305 Hartmann, J. F., Günthel, M., Klintzsch, T., Kirillin, G., Grossart, H. P., Keppler, F., and Isenbeck-Schröter, M.: High
306 spatiotemporal dynamics of methane production and emission in oxic surface water, *Environ Sci Technol*, 54, 1451–1463,
307 <https://doi.org/10.1021/acs.est.9b03182>, 2020.

308 Holmes, E. M., Sansone, F. J., Rust, T. M., and Popp, B. N.: Methane production, consumption, and air-sea exchange in the
309 open ocean: An evaluation based on carbon isotopic ratios, *Global Biogeochem Cycles*, 14, 1–10,
310 <https://doi.org/10.1029/1999GB001209>, 2000.

311 Holm-Hansen, O., Lorenzen, C. J., Holmes, R. W., and Strickland, J. D. H.: Fluorometric determination of chlorophyll, *Journal*
312 *du Conseil International pour L'Exploration de la Mer*, 30, 3–15, <https://doi.org/10.1093/icesjms/30.1.3>, 1965.

313 Igarza, M., Dittmar, T., Graco, M., and Niggemann, J.: Dissolved organic matter cycling in the coastal upwelling system off
314 central Peru during an “El Niño” year, *Front Mar Sci*, 6, 1–17, <https://doi.org/10.3389/fmars.2019.00198>, 2019.

315 IPCC: Climate change 2021: the physical science basis. Working Group I contribution to the IPCC sixth assessment report,
316 Cambridge University Press, 35–144 pp., 2021.

317 Jacob, B. G., Tapia, F. J., Quiñones, R. A., Montes, R., Sobarzo, M., Schneider, W., Daneri, G., Morales, C. E., Montero, P.,
318 and González, H. E.: Major changes in diatom abundance, productivity, and net community metabolism in a windier and dryer
319 coastal climate in the southern Humboldt Current, *Prog Oceanogr*, 168, 196–209,
320 <https://doi.org/10.1016/j.pocean.2018.10.001>, 2018.

321 Kara, A. B., Rochford, P. A., and Hurlburt, H. E.: Mixed layer depth variability over the global ocean, *J Geophys Res Oceans*,
322 108, 1–15, <https://doi.org/10.1029/2000jc000736>, 2003.

323 Karl, D. and Tilbrook, B.: Production and transport of methane in oceanic particulate organic matter, *Nature*, 368, 732–734,
324 1994.

325 Karl, D., Beversdorf, L., Björkman, K., Church, M., Martinez, A., and DeLong, E.: Aerobic production of methane in the sea,
326 *Nat Geosci*, 1, 473–478, <https://doi.org/10.1038/ngeo234>, 2008.

327 Klintzsch, T., Langer, G., Nehrke, G., Wieland, A., Lenhart, K., and Keppler, F.: Methane production by three widespread
328 marine phytoplankton species: release rates, precursor compounds, and relevance for the environment, *Biogeosciences*, 16,
329 4129–4144, <https://doi.org/10.5194/bg-2019-245>, 2019.

330 Klintzsch, T., Langer, G., Wieland, A., Geisinger, H., Lenhart, K., Nehrke, G., and Keppler, F.: Effects of temperature and
331 light on methane production of widespread marine phytoplankton, *J Geophys Res Biogeosci*, 125, 1–16,
332 <https://doi.org/10.1029/2020JG005793>, 2020.

333 Klintzsch, T., Geisinger, H., Wieland, A., Langer, G., Nehrke, G., Bizic, M., Greule, M., Lenhart, K., Borsch, C., Schroll, M.,
334 and Keppler, F.: Stable carbon isotope signature of methane released from phytoplankton, *Geophys Res Lett*, 50, 1–12,
335 <https://doi.org/10.1029/2023gl103317>, 2023.

336 Kock, A., Gebhardt, S., and Bange, H. W. W.: Methane emissions from the upwelling area off Mauritania (NW Africa),
337 *Biogeosciences*, 5, 1119–1125, <https://doi.org/10.5194/bg-5-1119-2008>, 2008.

138 De La Iglesia, R., Echenique-Subiabre, I., Rodríguez-Marconi, S., Espinoza, J. P., Von Dassow, P., Ulloa, O., and Trefault,
139 N.: Distinct oxygen environments shape picoeukaryote assemblages thriving oxygen minimum zone waters off central Chile,
140 J Plankton Res, 42, 514–529, <https://doi.org/10.1093/plankt/fbaa036>, 2020.

141 Lamontagne, R. A., Swinnerton, J. W., Linnenbom, V. J., and Smith, W. D.: Methane concentrations in various marine
142 environments, J Geophys Res, 78, 5317–5324, <https://doi.org/10.1029/JC078i024p05317>, 1973.

143 Lenhart, K., Klintzsch, T., Langer, G., Nehrke, G., Bunge, M., Schnell, S., and Keppler, F.: Evidence for methane production
144 by the marine algae *Emiliania huxleyi*, Biogeosciences, 13, 3163–3174, <https://doi.org/10.5194/bg-13-3163-2016>, 2016.

145 León-Palmero, E., Contreras-Ruiz, A., Sierra, A., Morales-Baquero, R., and Reche, I.: Dissolved CH₄ coupled to
146 photosynthetic picoeukaryotes in oxic waters and to cumulative chlorophyll a in anoxic waters of reservoirs, Biogeosciences,
147 17, 1–23, <https://doi.org/10.5194/bg-17-3223-2020>, 2020.

148 Li, J. and Dittrich, M.: [Dynamic polyphosphate metabolism in cyanobacteria responding to phosphorus availability](https://doi.org/10.1111/1462-2920.14488), Environ
149 Microbiol, 21, 572–583, <https://doi.org/10.1111/1462-2920.14488>, 2019.

150 Li, Y., Fichot, C. G., Geng, L., Scarratt, M. G., and Xie, H.: The contribution of methane photoproduction to the oceanic
151 methane paradox, Geophys Res Lett, 47, 1–10, <https://doi.org/10.1029/2020GL088362>, 2020.

152 Lidbury, I. D. E. A., Murrell, J. C., and Chen, Y.: Trimethylamine and trimethylamine N-oxide are supplementary energy
153 sources for a marine heterotrophic bacterium: Implications for marine carbon and nitrogen cycling, ISME Journal, 9, 760–769,
154 <https://doi.org/10.1038/ismej.2014.149>, 2015.

155 Llabrés, M., Agustí, S., and Herndl, G. J.: Diel in situ picophytoplankton cell death cycles coupled with cell division, J Phycol,
156 47, 1247–1257, <https://doi.org/10.1111/j.1529-8817.2011.01072.x>, 2011.

157 Lohrer, C., Cwierz, P. P., Wirth, M. A., Schulz-Bull, D. E., and Kanwischer, M.: Methodological aspects of methylphosphonic
158 acid analysis: Determination in river and coastal water samples, Talanta, 211, 1–8,
159 <https://doi.org/10.1016/j.talanta.2020.120724>, 2020.

160 Lu, X., Jacob, D. J., Zhang, Y., Maasakkers, J. D., Sulprizio, M. P., Shen, L., Qu, Z., Scarpelli, T. R., Nesser, H., Yantosca,
161 R. M., Sheng, J., Andrews, A., Parker, R. J., Boesch, H., Anthony Bloom, A., and Ma, S.: Global methane budget and trend,
162 2010-2017: Complementarity of inverse analyses using in situ (globalviewplus ch4 obspack) and satellite (gosat) observations,
163 <https://doi.org/10.5194/acp-21-4637-2021>, 25 March 2021.

164 Ma, X., Sun, M., Lennartz, S. T., and Bange, H. W.: A decade of methane measurements at the Boknis Eck Time-series Station
165 in the Eckernförde Bay (Southwestern Baltic Sea), Biogeosciences Discussions, 2020, 1–22, <https://doi.org/10.5194/bg-2020-107>, 2020.

166
167 Mao, S. H., Zhang, H. H., Zhuang, G. C., Li, X. J., Liu, Q., Zhou, Z., Wang, W. L., Li, C. Y., Lu, K. Y., Liu, X. T., Montgomery,
168 A., Joye, S. B., Zhang, Y. Z., and Yang, G. P.: Aerobic oxidation of methane significantly reduces global diffusive methane
169 emissions from shallow marine waters, Nat Commun, 13, <https://doi.org/10.1038/s41467-022-35082-y>, 2022.

Formatted: Subscript

370 Martínez, A., Ventouras, L. A., Wilson, S. T., Karl, D. M., and DeLong, E. F.: Metatranscriptomic and functional metagenomic
371 analysis of methylphosphonate utilization by marine bacteria, *Front Microbiol*, 4, <https://doi.org/10.3389/fmicb.2013.00340>,
372 2013.

373 McAuliffe, C.: Solubility in water of C1-C9 hydrocarbons, *Nature*, 200, 1092–1093, 1963.

374 McClain, M. E., Boyer, E. W., Dent, C. L., Gergel, S. E., Grimm, N. B., Groffman, P. M., Hart, S. C., Harvey, J. W., Johnston,
375 C. A., Mayorga, E., McDowell, W. H., and Pinay, G.: Biogeochemical Hot Spots and Hot Moments at the Interface of
376 Terrestrial and Aquatic Ecosystems, <https://doi.org/10.1007/s10021-003-0161-9>, June 2003.

377 Metcalf, W. W., Griffin, B. M., Cicchillo, R., Gao, J., Janga, S., Cooke, H., Circello, B., Evans, B., Martens-Habbena, W.,
378 Stahl, D., and Van Der Donk, W.: Synthesis of methylphosphonic acid by marine microbes: a source for methane in the
379 Aerobic Ocean, *Science* (1979), 337, 1104–1107, <https://doi.org/10.1126/science.1219875>, 2012.

380 Minor, E. C., Swenson, M. M., Mattson, B. M., and Oyler, A. R.: Structural characterization of dissolved organic matter: A
381 review of current techniques for isolation and analysis, *Environmental Sciences: Processes and Impacts*, 16, 2064–2079,
382 <https://doi.org/10.1039/c4em00062e>, 2014.

383 Molina, V., Belmar, L., Levipan, H. A., Ramírez-Flandes, S., Anguita, C., Galán, A., Montes, I., and Ulloa, O.: Spatiotemporal
384 distribution of key pelagic microbes in a seasonal oxygen-deficient coastal upwelling system of the Eastern South Pacific
385 Ocean, *Front Mar Sci*, 7, 1–17, <https://doi.org/10.3389/fmars.2020.561597>, 2020.

386 Mopper, K., Kieber, D. J., and Stubbins, A.: Marine photochemistry of organic matter: processes and impacts. processes and
387 impacts., in: *Biogeochemistry of Marine Dissolved Organic Matter: Second Edition*, Elsevier Inc., 389–450,
388 <https://doi.org/10.1016/B978-0-12-405940-5.00008-X>, 2015.

389 Morales, C. and Anabalón, V.: Phytoplankton biomass and microbial abundances during the spring upwelling season in the
390 coastal area off Concepción , central-southern Chile : variability around a time series station, *Prog Oceanogr*, 92–95, 81–91,
391 <https://doi.org/10.1016/j.pocean.2011.07.004>, 2012.

392 Morales, C., González, H. E., Hormazabal, S. E., Yuras, G., Letelier, J., and Castro, L. R.: The distribution of chlorophyll- a
393 and dominant planktonic components in the coastal transition zone off Concepción, central Chile, during different
394 oceanographic conditions, *Prog Oceanogr*, 75, 452–469, <https://doi.org/10.1016/j.pocean.2007.08.026>, 2007.

395 Morán, X. A. G., Estrada, M., Gasol, J. M., and Pedrós-Alió, C.: Dissolved primary production and the strength of
396 phytoplankton-bacterioplankton coupling in contrasting marine regions, *Microb Ecol*, 44, 217–223,
397 <https://doi.org/10.1007/s00248-002-1026-z>, 2002.

398 Morana, C., Bouillon, S., Nolla-Ardèvol, V., Roland, F., Okello, W., Descy, J.-P., Nankabirwa, A., Nabafu, E., Springael, D.,
399 and Borges, A.: Methane paradox in tropical lakes? Sedimentary fluxes rather than water column production in oxic waters
000 sustain methanotrophy and emissions to the atmosphere, *Biogeosciences Discussions*, 17, 1–20, [https://doi.org/10.5194/bg-](https://doi.org/10.5194/bg-2020-142)
001 2020-142, 2020.

002 Muñoz-Marín, M. C., Gómez-Baena, G., López-Lozano, A., Moreno-Cabezuelo, J. A., Díez, J., and García-Fernández, J. M.:
003 Mixotrophy in marine picocyanobacteria: use of organic compounds by *Prochlorococcus* and *Synechococcus*,
004 <https://doi.org/10.1038/s41396-020-0603-9>, 1 May 2020.

005 Oremland, R. S.: Methanogenic activity in plankton samples and fish intestines: A mechanism for in situ methanogenesis in
006 oceanic surface waters, *Limnol. Oceanogr.*, 24, 1136–1141, 1979.

007 Paul, L., Ferguson, D. J., and Krzycki, J. A.: The trimethylamine methyltransferase gene and multiple dimethylamine
008 methyltransferase genes of *methanosarcina barkeri* contain in-frame and read-through amber codons, *J Bacteriol*, 182, 2520–
009 2529, [https://doi.org/0021-9193/00/\\$04.00](https://doi.org/0021-9193/00/$04.00)≤0, 2000.

010 Rain-Franco, A., Sobarzo, M., Caparros, J., and Fernandez, C.: Variability of chromophoric dissolved organic matter in three
011 freshwater-influenced systems along central-southern Chile, *Prog Oceanogr*, 174, 154–161,
012 <https://doi.org/10.1016/j.pocean.2018.09.009>, 2019.

013 Raven, J. A.: The twelfth tansley lecture. Small is beautiful: the picophytoplankton, *Funct Ecol*, 12, 503–513,
014 <https://doi.org/10.1046/j.1365-2435.1998.00233.x>, 1998.

015 Reeburgh, W. S.: Oceanic methane biogeochemistry, *American Chemical Society*, 107, 486–513,
016 <https://doi.org/10.1021/cr050362v>, 2007.

017 Reintjes, G., Fuchs, B. M., Scharfe, M., Wiltshire, K. H., Amann, R., and Arnosti, C.: Short-term changes in polysaccharide
018 utilization mechanisms of marine bacterioplankton during a spring phytoplankton bloom, *Environ Microbiol*, 22, 1884–1900,
019 <https://doi.org/10.1111/1462-2920.14971>, 2020.

020 Repeta, D. J., Ferrón, S., Sosa, O. A., Johnson, C. G., Repeta, L. D., Acker, M., DeLong, E. F., and Karl, D. M.: Marine
021 methane paradox explained by bacterial degradation of dissolved organic matter, *Nat Geosci*, 9, 1–7,
022 <https://doi.org/10.1038/ngeo2837>, 2016.

023 Roth, F., Sun, X., Geibel, M. C., Prytherch, J., Brüchert, V., Bonaglia, S., Broman, E., Nascimento, F., Norkko, A., and
024 Humborg, C.: High spatiotemporal variability of methane concentrations challenges estimates of emissions across vegetated
025 coastal ecosystems, *Glob Chang Biol*, <https://doi.org/10.1111/gcb.16177>, 2022.

026 Saunio, M., Stavert, A. R., Poulter, B., Bousquet, P., Canadell, J. G., Jackson, R. B., Raymond, P. A., Dlugokencky, E. J.,
027 and Houweling, S.: The global methane budget 2000 – 2017, *Earth Syst Sci Data*, 12, 1561–1623, [https://doi.org/10.5194/essd-](https://doi.org/10.5194/essd-12-1561-2020)
028 [12-1561-2020](https://doi.org/10.5194/essd-12-1561-2020), 2020.

029 Schlitzer, R.: *Ocean Data View*, 2023.

030 [Schowanek, D. and Verstraete, W.: Phosphonate utilization by bacteria in the presence of alternative phosphorus sources,](#)
031 [Biodegradation, Kluwer Academic Publishers, 1990 pp., 1990.](#)

032 Sieburth, J., Smetacek, V., and Lenz, J.: Pelagic ecosystem structure: Heterotrophic compartments of the plankton and their
033 relationship to plankton size fractions, *Limnol. Oceanogr.*, 23, 1256–1263, <https://doi.org/10.4319/lo.1978.23.6.1256>, 1978.

134 Smith, M. W., Allen, L. Z., Allen, A. E., Herfort, L., and Simon, H. M.: Contrasting genomic properties of free-living and
135 particle-attached microbial assemblages within a coastal ecosystem, *Front Microbiol*, 4, 1–20,
136 <https://doi.org/10.3389/fmicb.2013.00120>, 2013.

137 Sobarzo, M. and Djurfeldt, L.: Coastal upwelling process on a continental shelf limited by submarine canyons, Concepción,
138 central Chile, *J Geophys Res*, 109, 1–20, <https://doi.org/10.1029/2004JC002350>, 2004.

139 Sobarzo, M., Bravo, L., Donoso, D., Garcés-Vargas, J., and Schneider, W.: Coastal upwelling and seasonal cycles that
140 influence the water column over the continental shelf off central Chile, *Prog Oceanogr*, 75, 363–382,
141 <https://doi.org/10.1016/j.pocean.2007.08.022>, 2007.

142 Sosa, O. A., Repeta, D. J., DeLong, E. F., Ashkezari, M. D., and Karl, D. M.: Phosphate-limited ocean regions select for
143 bacterial populations enriched in the carbon–phosphorus lyase pathway for phosphonate degradation, *Environ Microbiol*, 21,
144 2402–2414, <https://doi.org/10.1111/1462-2920.14628>, 2019.

145 Sosa, O. A., Burrell, T. J., Wilson, S. T., Foreman, R. K., Karl, D. M., and Repeta, D. J.: Phosphonate cycling supports methane
146 and ethylene supersaturation in the phosphate-depleted western North Atlantic Ocean, *Limnol Oceanogr*, 1–17,
147 <https://doi.org/10.1002/lno.11463>, 2020.

148 Spilling, K., Camarena-Gómez, M. T., Lipsowers, T., Martínez-Varela, A., Díaz-Rosas, F., Eronen-Rasimus, E., Silva, N., von
149 Dassow, P., and Montecino, V.: Impacts of reduced inorganic N:P ratio on three distinct plankton communities in the Humboldt
150 upwelling system, *Mar Biol*, 166, 1–17, <https://doi.org/10.1007/s00227-019-3561-x>, 2019.

151 Stefels, J. and Van Boekel, W.: Production of DMS from dissolved DMSP in axenic cultures of the marine phytoplankton
152 species *Phaeocystis* sp, *Mar Ecol Prog Ser*, 97, 11–18, <https://doi.org/https://www.jstor.org/stable/24833593>, 1993.

153 Strub, T., Mesias, J., Montecino, V., Rutllant, J., and Salinas, S.: Coastal ocean circulation off western south america, in: *The*
154 *global coastal ocean - regional studies and syntheses*, vol. 11, 273–313, 1998.

155 Sun, J., Steindler, L., Thrash, J. C., Halsey, K. H., Smith, D. P., Carter, A. E., Landry, Z. C., and Giovannoni, S. J.: One carbon
156 metabolism in SAR11 pelagic marine bacteria, *PLoS One*, 6, 1–12, <https://doi.org/10.1371/journal.pone.0023973>, 2011.

157 Sun, J., Mausz, M. A., Chen, Y., and Giovannoni, S. J.: Microbial trimethylamine metabolism in marine environments, *Environ*
158 *Microbiol*, 21, 513–520, <https://doi.org/10.1111/1462-2920.14461>, 2019.

159 Taenzer, L.: *The isotope biogeochemistry of methane produced from the C-P lyase pathway*, Dartmouth College, 2019.

160 Testa, G., Masotti, I., and Fariás, L.: Temporal variability in net primary production in an upwelling area off central Chile
161 (36°S), *Front Mar Sci*, 5, 1–17, <https://doi.org/10.3389/fmars.2018.00179>, 2018.

162 Upstill-goddard, R. C. and Barnes, J.: Methane emissions from UK estuaries: Re-evaluating the estuarine source of
163 tropospheric methane from Europe, 180, 14–23, <https://doi.org/10.1016/j.marchem.2016.01.010>, 2016.

164 Urata, S., Kurosawa, Y., Yamasaki, N., Yamamoto, H., Nishiwaki, N., Hongo, Y., Adachi, M., and Yamaguchi, H.: Utilization
165 of phosphonic acid compounds by marine bacteria of the genera *Phaeobacter*, *Ruegeria*, and *Thalassospira* (α -Proteobacteria),
166 *FEMS Microbiol Lett*, 369, <https://doi.org/10.1093/femsle/fnac065>, 2022.

167 Del Valle, D. A. and Karl, D. M.: Aerobic production of methane from dissolved water-column methylphosphonate and sinking
168 particles in the North Pacific Subtropical Gyre, *Aquatic Microbial Ecology*, 73, 93–105, <https://doi.org/10.3354/ame01714>,
169 2014.

170 Vargas, C. A., Martínez, R. A., Cuevas, L. A., Pavez, M. A., Cartes, C., González, H. E., Escribano, R., and Daneri, G.: The
171 relative importance of microbial and classical food webs in a highly productive coastal upwelling area, *Limnol Oceanogr*, 52,
172 1495–1510, <https://doi.org/10.4319/lo.2007.52.4.1495>, 2007.

173 Vargas, C. A., Arriagada, L., Sobarzo, M., Contreras, P. Y., and Saldías, G.: Bacterial production along a river-to-ocean
174 continuum in central Chile: implications for organic matter cycling, *Aquatic Microbial Ecology*, 68, 195–213,
175 <https://doi.org/10.3354/ame01608>, 2013.

176 Vargas, C. A., Contreras, P. Y., Pérez, C. A., Sobarzo, M., Saldías, G. S., and Salisbury, J.: Influences of riverine and upwelling
177 waters on the coastal carbonate system off Central Chile and their ocean acidification implications, *J Geophys Res Biogeosci*,
178 121, 1–16, <https://doi.org/10.1002/2015JG003213>, 2016.

179 Wang, Q., Dore, J. E., and McDermott, T. R.: Methylphosphonate metabolism by *Pseudomonas* sp. populations contributes to
180 the methane oversaturation paradox in an oxic freshwater lake, *Environ Microbiol*, 19, 1–41, [https://doi.org/10.1111/1462-](https://doi.org/10.1111/1462-2920.13747)
181 [2920.13747](https://doi.org/10.1111/1462-2920.13747), 2018.

182 Wang, Q., Alowaiifeer, A., Kerner, P., Balasubramanian, N., Patterson, A., Christian, W., Tarver, A., Dore, J. E., Hatzenpichler,
183 R., Bothner, B., and McDermott, T. R.: Aerobic bacterial methane synthesis, *Proceedings of the National Academy of*
184 *Sciences*, 118, 1–9, <https://doi.org/10.1073/pnas.2019229118>, 2021.

185 Wanninkhof, R.: Relationship between wind speed and gas exchange over the ocean, *J Geophys Res*, 97, 7373–7382,
186 <https://doi.org/10.1029/92JC00188>, 1992.

187 Weber, T., Wiseman, N. A., and Kock, A.: Global ocean methane emissions dominated by shallow coastal waters, *Nat*
188 *Commun*, 10, 1–10, <https://doi.org/10.1038/s41467-019-12541-7>, 2019.

189 Wiesenburg, D. A. and Guinasso, N. L.: Equilibrium solubilities of methane, carbon monoxide, and hydrogen in water and sea
190 water, *American Chemical Society*, 24, 356–360, 1979.

191 Worden, A.: Picoeukaryote diversity in coastal waters of the Pacific Ocean, *Aquatic microbial ecology*, 43, 165–175,
192 <https://doi.org/doi:10.3354/ame043165>, 2006.

193 Xu, S., Sun, Z., Geng, W., Cao, H., Zhang, X., Zhai, B., and Wu, Z.: Advance in Numerical Simulation Research of Marine
194 Methane Processes, *Front Earth Sci (Lausanne)*, 10, <https://doi.org/10.3389/feart.2022.891393>, 2022.

195 Ye, W. W., Wang, X. L., Zhang, X.-H., and Zhang, G.-L.: Methane production in oxic seawater of the western North Pacific
196 and its marginal seas, *Limnol Oceanogr*, 65, 1–14, <https://doi.org/10.1002/lno.11457>, 2020.

197 Zhang, Y. and Xie, H.: Photomineralization and photomethanification of dissolved organic matter in Saguenay River surface
198 water, *Biogeosciences*, 12, 6823–6836, <https://doi.org/10.5194/bg-12-6823-2015>, 2015.

199 Zhao, L., Lin, L.-Z., Chen, M.-Y., Teng, W.-K., Zheng, L.-L., Peng, L., Lv, J., Brand, J. J., Hu, C.-X., Han, B.-P., Song, L.-
100 R., and Shu, W.-S.: The widespread capability of methylphosphonate utilization in filamentous cyanobacteria and its
101 ecological significance, *Water Res*, 217, 1–11, <https://doi.org/10.1016/j.watres.2022.118385>, 2022.

102